A two-and-half dimensional finite element/boundary element model for predicting the vibro-acoustic behaviour of panels with poro-elastic media

Tiesong Deng [a], Xiaozhen Sheng [b*], Hongseok Jeong [c], David J. Thompson [c]

[a] *State Key Laboratory of Traction Power, Southwest Jiaotong University, Chengdu, China*

[b] *School of Urban Railway Transportation, Shanghai University of Engineering Science, Shanghai, China*

[c] *Institute of Sound and Vibration Research, University of Southampton, Southampton, UK*

[*] *Correponding author. E-mail address: shengxiaozhen@hotmail.com*

Abstract

Solid panels with additional poro-elastic materials are widely used in engineering, mainly for sound insulation. In many cases, the panels are constructed in such a way that they can be idealised to be infinitely long and uniform in one direction, forming a so-called two-and-a-half dimensional (2.5D) structure. Although the 2.5D finite element and boundary element methods (FEM-BEM) are particularly suitable for predicting the vibro-acoustic behaviour of such structures, up to now the presence of poro-elastic media have not been adequately considered. In this paper a 2.5D FE-BE vibro-acoustic model is presented which accounts for solids, fluids and poro-elastic media. The poro-elastic media are modelled using the 2.5D FE approach based on the mixed displacement-pressure formulation of Biot's theory. The solids are also modelled using the 2.5D FE method but based on the linear theory of elasticity. The internal fluids are modelled using the 2.5D FE method as well. For a flat panel, the external fluid on both sides of the panel can be modelled using the 2.5D BE method based on the Rayleigh integral. The coupling between the various sub-models is derived in detail. The accuracy of the model is demonstrated by applying it to simple multi-layered structures for which solutions can be produced using other well-established methods. It is demonstrated that the elasticity of the solid frame of a porous medium has a great influence on the vibro-acoustics of a structure containing the porous material. The method is then applied to investigate the sound transmission loss (STL) of a typical railway vehicle floor structure. Results show that STL can be greatly improved by proper arrangement of porous material layers between the interior wooden floor and the outer extrusion; however, the load bearing supporting beams may significantly reduce the benefit of the porous material layers.

Keywords: Transmission loss; poro-elastic panel; 2.5D finite element method; 2.5D boundary

element method

1. Introduction

Nowadays, solid panels with additional poro-elastic materials are widely used in engineering such as railway vehicles, ships, aircraft and automobiles for their sound absorption, sound insulation and vibration mitigation [1]. To design such panels at an early stage, their vibro-acoustic behaviour needs to be predicted.

Analytical approaches can be used to predict the vibro-acoustic behaviour of simple structures. Applications of analytical approaches can be found for an orthogonally rib-stiffened sandwich structure [2], a corrugated core sandwich structure [3], a periodically rib-stiffened double-panel [4] and a sandwich structure with two-layered pyramidal cores [5]. A common feature of these structures is that the ribs or cores are periodically distributed and these structures are either filled [2][3][5] or laminated [4] with porous materials. Depending on the rigidity and weight of the porous medium considered, the porous material can be simplified as an equivalent fluid having an effective density and bulk modulus [2][3][4], or be treated as a poro-elastic medium having an elastic frame based on Biot's theory [5]. The ribs can be modelled with beams [4] or replaced with translational and rotational springs [2][3][5]. Due to the periodic distribution of the ribs or cores, the spatial harmonics approach is used to determine sound radiation and sound insulation of the panel. For a rectangular plate treated with a layer of porous material, Zhang and Sheng [6] used a measured or predicted surface impedance to replace the porous material layer, ignoring the bending vibration of the porous medium and interaction between the porous material layer and the back plate. This approach may cause significant errors in the prediction of sound transmission loss (STL) when the porous layer is not sufficiently light, thin and soft. In most of these analytical approaches, the panel is assumed to be infinite, ignoring the presence of any boundary.

If the structures are complicated with irregularly distributed ribs or cores, the abovementioned analytical approaches cannot be used. In this case, the conventional finite element method (FEM) and boundary element method (BEM) may be combined to determine the sound radiation and STL of such panels. To account for sound absorbing media, numerous FE models have been developed [7]-[13]. They are mainly based on impedance techniques [7], poro-rigid models [8] or the classical Biot's displacement (u, U) theory [9]-[13]. The models in Refs. [7][8] are simple approaches which

neglect the vibration and mass of the solid frame whereas the use of Biot's theory in the models of Refs. [9]-[13] is a more comprehensive approach. In Biot's theory [14][15], the elasticity of the solid frame and the inertial coupling between the solid frame and the interstitial fluid are considered. For the general application in which sound absorbing materials, often attached to, or filled in the cavities of, a structure, vibrate together with the structure, the use of Biot's theory becomes necessary. However, such approaches have the disadvantage that the corresponding matrices are implicitly frequency-dependent, requiring reconstruction at each frequency in a spectral analysis. Moreover, they have six degrees of freedom at each node, three components for the solid displacement vector (u) and three components for the fluid displacement vector (U). These disadvantages limit their computational efficiency.

To compensate for these difficulties, an exact mixed displacement-pressure (u, p) formulation has been developed from the classical (u, U) theory [16]-[19]. In the formulation, the Biot's poro-elasticity equations are rewritten in terms of the solid phase displacement vector (u) and the interstitial fluid phase pressure (p) [16][17]. Based on the weak integrals of the equations governing (u, p), a 3D FE model has been developed by Atalla et al. [18][19]. This method has only four degrees of freedom at each node, making it more efficient and easier to model the poro-elastic media using classical FEM codes. It should be noted that the corresponding FE matrices depend explicitly on frequency. The boundary conditions of the (u, p) formulation, described in Ref. [20], are combined with the surface integrals of the associated weak integral forms to account for exterior excitation, supports and coupling with acoustic, elastic and/or poro-elastic media. However, the mixed displacement-pressure FE approach, while accurate and efficient compared with the displacement (u, U) formulation, may also lead to considerable computational costs arising from the large size and complexity of the structure and mesh requirements for reasonable results.

In many cases, the structure is constructed in such a way that it can be idealised to be infinitely long and uniform in one direction (the longitudinal direction), forming a so-called two-and-a-half dimensional (2.5D) structure. The 2.5D FE and BE methods (2.5D FE-BE method) are particularly suitable for predicting the vibro-acoustic behaviour of a 2.5D structure [21]-[25]. For example, Prasetiyo [22] used this method to study the STL of an infinitely long plate. Accuracy of the method is demonstrated by comparing it to an analytical model. Nillson et al. [23], using the 2.5D FE-BE method, studied the effect of a damping rubber layer on the STL of a typical truss-core extrusion

from high-speed train floors. STL optimisation was performed by Zhang et al. in Ref. [24] for an extrusion using the 2.5D FE-BE method through a parametric study. Sound radiation behaviour of the extrusion was investigated by Kim et al. [25].

In practical usage, a high-speed train floor consists of an exterior truss-core extrusion, layers of porous materials (the acoustic treatment) and an interior wooden floor. To bear the weight inside the train carriage, wooden beams are installed between the extrusion and the wooden floor. Deng et al. [26] ignored the presence of the wooden beams and established a vibro-acoustic model to study the influence of the acoustic treatment on the composite structure. In the model, the acoustic treatment is assumed to be unbounded in both the longitudinal and lateral directions and layered, and a two-dimensional Fourier transformed transfer matrix method (TMM) is used to model the vibro-acoustic response of the acoustic treatment and the fluid domain containing the transmitted sound waves; the 2.5D FE-BE method is used to deal with that of the extrusion and the fluid domain containing the incident and reflected sound waves. The coupling between the acoustic treatment and the extrusion is formulated based on the stress balance and displacement continuity at the interface. However, if the wooden beams are considered, the model developed in Ref. [26] is no longer applicable. For such a composite structure, a complete 2.5D FE-BE model is desirable. Unfortunately, the 2.5D FE-BE-based models developed so far have not considered the presence of poro-elastic media.

The aim of this paper is to present a 2.5D FE-BE model which can couple the poro-elastic medium with elastic solids and acoustic media; the model was initially developed and applied to analyse the sound radiation and absorption of railway track structures in Ref. [27], the PhD thesis of the third author of the current paper. The model in Ref. [27] is extended in the current work by including the coupling between the 2.5D FE models of two different sound absorbing materials, and applied to predict the STL of composite structures which are much more complex than the railway track structure considered in Ref. [27].

The formulation of the model is presented in Section 2 with a detailed description of 2.5D FE modelling for poro-elastic media and couplings between 2.5D FE models of solids, internal fluids and other poro-elastic media. Coupling with 2.5D BE models of the external acoustic fluids are also described in this section, resulting in a global 2.5D FE-BE model. In Section 3, the 2.5D FE-BE model is applied to study the vibro-acoustics of panels having a layered structure, for demonstrating

the accuracy and effectiveness of the model by comparing with other methods, mostly TMM. In Section 4, the model is then applied to investigate the sound transmission loss of a typical railway vehicle structure.

2. Formulation

In many engineering applications, flat structures, including those with additional poro-elastic media, solids or internal acoustic fluids and surrounded by external acoustic domains, are often long and uniform in the longitudinal (*x*-) direction. At high frequencies, where the acoustic and structural wavelengths are shorter than the longitudinal dimension, the structure can be idealized to be infinitely long in that direction but bounded in the *y*-*z* plane, forming a so-called 2.5D structure, as shown in Fig. 1. The cross-section of the structure can be formed with solids, fluids and poro-elastic media, as exemplified by a multi-layered panel (Fig. 2(a)) and a rib-stiffened panel with cavities filled with other media (Fig. 2(b)).

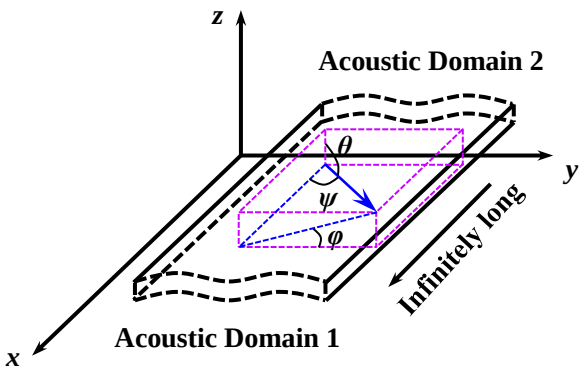

Fig. 1 A sketch of a 2.5D panel

(a) (b)

Fig. 2 Two cross-section examples. (a) A multi-layered panel; (b) A rib-stiffened panel filled with other media.

It is assumed that the structure is in an unbounded baffle separating the whole space into two acoustic domains (acoustic domain 1 and acoustic domain 2). A plane wave in acoustic domain 1 is incident upon the structure at angles φ and ψ, as defined in Fig. 1; The angle of the wave vector relative to the *z*-axis is given by $\theta = \arccos\left(\sin\psi \sin\varphi\right)$. The incident wave at radian frequency ω can be expressed as

$$p_{\mathrm{i}}(x,y,z,t) = \bar{p}_{\mathrm{i}}\, \mathrm{e}^{-\mathrm{i}k_x x} \mathrm{e}^{-\mathrm{i}k_y y} \mathrm{e}^{-\mathrm{i}k_z z} \mathrm{e}^{\mathrm{i}\omega t} \tag{1}$$

where $\bar{p}_{\mathrm{i}}$ is the sound pressure amplitude, $\mathrm{i}=\sqrt{-1}$, and

$$k_x = k_1 \cos\psi\,, \quad k_y = k_1 \sin\psi\cos\varphi\,, \quad k_z = k_1 \sin\psi\sin\varphi \tag{2}$$

are wavenumbers in the *x*-, *y*- and *z*-direction, with k_1 being the acoustic wavenumber in acoustic domain 1. As the structure is flexible, the incident wave will be partly reflected back to acoustic domain 1 and partly transmitted into acoustic domain 2, generating a reflected wave and a transmitted wave. The 2.5D FE-BE method, which fully makes use of the uniformity and infinity of the structure in the *x*-direction, is particularly suitable for predicting these reflected and transmitted waves. The model generated from the 2.5D FE-BE method is formed by a number of sub-models which are coupled together by interface conditions between the structure components. The sub-models include 2.5D FE models for the solids and the internal acoustic fluids, 2.5D BE models for the exterior acoustic domains, and 2.5D FE models for the poro-elastic media.

Since 2.5D FE/BE modelling for solids and fluids is well established and the details can be found in the literature, the 2.5D FE models for the solids and the internal acoustic fluids, the 2.5D BE models for the exterior acoustic domains, and the coupling of these sub-models are only briefly introduced in Section 2.1. Greater efforts are given in Section 2.2 to the formulation of the 2.5D FE model for a poro-elastic medium. Coupling between the poro-elastic medium 2.5D FE model and other sub-models are formulated in Section 2.3. The final global model for the structure is given in Section 2.4.

2.1 2.5D FE/BE models for solids and fluids and the coupling

It is assumed that the vibro-acoustics of the structure is temporally harmonic at radian frequency ω. Since the structure and acoustic domains are infinitely long in the *x*-direction, the amplitude, $\bar{f}(x,y,z)$, of any quantity can be expressed as an inverse Fourier transform

$$\bar{f}(x,y,z) = \frac{1}{2\pi}\int_{-\infty}^{+\infty} \tilde{f}(\beta,y,z)\mathrm{e}^{\mathrm{i}\beta x}\mathrm{d}\beta\,, \tag{3}$$

where $\tilde{f}(\beta,y,z)$ is the Fourier transform of $\bar{f}(x,y,z)$. Physically, Eq. (3) indicates that $\bar{f}(x,y,z)$ is superposition of waves propagating in the *x*-direction at particular wavenumbers denoted by β. Since the geometry and material property of the structure is invariant with *x*, the differential equations defined in the three-dimensional space and governing the vibro-acoustics of the structure

can be reduced to be defined in the two-dimensional *y*-*z* plane using Eq. (3) with the wavenumber β as a parameter. For a given value of β, these two-dimensional differential equations may be solved following the finite element method, resulting in a 2.5D FE model or 2.5D FE equation (the term 2.5D is used since responses in *x*-, *y*- and *z*-directions are determined based on a two-dimensional mesh in the *y*-*z* plane), or the boundary element method, resulting in a 2.5D BE model or 2.5D BE equation. In what follows, $\tilde{f}(\beta, y, z)$ and $\bar{f}(x, y, z)$ are called by the same physical terminology, although they have different units.

For an elastic solid (indicated by subscript e) in the structure, a vibration wave at radian frequency ω and wavenumber β in the *x*-direction (Fig. 1) can be described by the so called 2.5D FE equation derived based on the linear theory of elasticity [25][28]. The equation is given by

$$\left[\mathbf{K}_{\mathrm{e}}(\beta) - \omega^2 \mathbf{M}_{\mathrm{e}}\right]\tilde{\mathbf{u}}_{\mathrm{e}} = \tilde{\mathbf{F}}_{\mathrm{e}}, \tag{4}$$

where

$$\mathbf{K}_{\mathrm{e}}(\beta) = (-\mathrm{i}\beta)^4 \mathbf{K}_{\mathrm{e4}} + (-\mathrm{i}\beta)^2 \mathbf{K}_{\mathrm{e2}} + (-\mathrm{i}\beta)\mathbf{K}_{\mathrm{e1}} + \mathbf{K}_{\mathrm{e0}}, \tag{5}$$

in which $\mathbf{K}_{\mathrm{e0}}$, $\mathbf{K}_{\mathrm{e1}}$, $\mathbf{K}_{\mathrm{e2}}$ and $\mathbf{K}_{\mathrm{e4}}$ are related to the stiffness of the elastic solid. $\mathbf{K}_{\mathrm{e4}} \neq \mathbf{0}$ if 2.5D shell elements (i.e., elements having both translational nodal displacements and rotational nodal displacement) are used and $\mathbf{K}_{\mathrm{e4}} = \mathbf{0}$ if 2.5D solid elements (i.e., elements only having translational nodal displacements) are used. $\mathbf{M}_{\mathrm{e}}$ is the mass matrix. $\tilde{\mathbf{u}}_{\mathrm{e}}$ represents the vector of nodal displacement amplitudes and $\tilde{\mathbf{F}}_{\mathrm{e}}$ is the associated vector of nodal force amplitudes. Note that the nodal displacements are in units m/(rad/m) and the nodal forces in units (N/m)/(rad/m). For the case shown in Fig. 1, nodal forces may be contributed by the acoustic waves in the two acoustic domains, and/or by other parts of the structure.

The interior acoustic fluid in the structure can also be modelled using the 2.5D FE method as detailed in Refs. [25][28], but the equation takes the form of (subscript a is used to indicate air)

$$\left[\frac{1}{\omega^2}\mathbf{K}_{\mathrm{a}}(\beta) - \mathbf{M}_{\mathrm{a}}\right]\tilde{\mathbf{p}}_{\mathrm{a}} = \tilde{\mathbf{F}}_{\mathrm{a}}, \tag{6}$$

where

$$\mathbf{K}_{\mathrm{a}}(\beta) = (-\mathrm{i}\beta)^2 \mathbf{K}_{\mathrm{a2}} + \mathbf{K}_{\mathrm{a0}}, \tag{7}$$

in which $\mathbf{K}_{a2}$ and $\mathbf{K}_{a0}$ correspond to the 'mass' matrices of the internal fluid and $\mathbf{M}_a$ is the 'stiffness' matrix. $\tilde{\mathbf{p}}_a$ is the vector of nodal sound pressure amplitudes, and $\tilde{\mathbf{F}}_a$ is the associated vector of nodal force amplitudes.

The exterior acoustic fluid on both sides of the structure can be dealt with using the 2.5D BE method as detailed in Refs. [26][28]

$$\mathbf{H}_a(\beta)\tilde{\mathbf{p}}_a - \mathbf{G}_a(\beta)\tilde{\mathbf{v}}_{an} = \mathbf{0}, \tag{8}$$

where $\mathbf{G}_a$ and $\mathbf{H}_a$ are two BE matrices; $\tilde{\mathbf{p}}_a$ and $\tilde{\mathbf{v}}_{an}$ are the vectors of nodal pressure and normal velocity amplitudes at the (acoustic domain/structure) interface. When the structure is flat (i.e. it is a panel) and mounted in a co-planar baffle on both sides, the 2.5D boundary integral equation from which Eq. (8) is derived reduces to the 2.5D Rayleigh integral [29]. Boundary element equation can be similarly established based on the 2.5D Rayleigh integral and takes the same form as Eq. (8) but with the matrix $\mathbf{H}_a$ being a unit matrix. In the Rayleigh integral, only the vibration of the wetting surface of the structure is needed and therefore the computation efficiency is improved and the errors arising from the boundary truncation on the semi-infinite baffles when using the full-space Green's functions (full-space Green's functions are normally used in boundary element method) can be avoided [28].

On the interface of the elastic solid and the internal acoustic fluid, vibrational velocity and stress (traction) in the direction normal to the interface are continuous. These interface conditions can be described mathematically by (the tensor summation convention is used)

$$\begin{cases} \sigma_{ij}^{e} n_j = -p_a \delta_{ij} n_j \\ u_i^{e} n_i = u_{an} = \dfrac{1}{\rho_0 \omega^2} \dfrac{\partial p_a}{\partial \mathbf{n}} \end{cases}, \tag{9}$$

where $\mathbf{n}$ is the unit normal vector on the interface, pointing out of the elastic solid, σ_{ij}^{e} and u_i^{e} are the stress tensor and ith displacement component of the elastic solid, ρ_0 and p_a are the density and sound pressure of the internal fluid. With Eq. (9), the tractions at the interface can be transformed to equivalent nodal forces for the elastic solid and the internal acoustic fluid, resulting in two coupling matrices $\mathbf{C}_{ea}$ and $\mathbf{C}_{ae}$, where $\mathbf{C}_{ea} = \mathbf{C}_{ae}^{T}$. Therefore, by combining Eqs. (4) and (6), the governing equation of the coupled solid and fluid is given,

$$\begin{bmatrix} \mathbf{K}_{\mathrm{e}}(\beta)-\omega^2\mathbf{M}_{\mathrm{e}} & \mathbf{C}_{\mathrm{ea}} \\ \mathbf{C}_{\mathrm{ae}} & \frac{1}{\omega^2}\mathbf{K}_{\mathrm{a}}(\beta)-\mathbf{M}_{\mathrm{a}} \end{bmatrix} \begin{pmatrix} \tilde{\mathbf{u}}_{\mathrm{e}} \\ \tilde{\mathbf{p}}_{\mathrm{a}} \end{pmatrix} = \begin{pmatrix} \tilde{\mathbf{F}}_{\mathrm{e}} \\ \tilde{\mathbf{F}}_{\mathrm{a}} \end{pmatrix}, \tag{10}$$

Similarly, an elastic solid is coupled with an external acoustic fluid by combining Eqs. (4) and (8) and the associated interface conditions, resulting in

$$\begin{bmatrix} \mathbf{I}_{\mathrm{ae}} & \mathbf{0} & -\mathrm{i}\omega\mathbf{E}_{\mathrm{e}} \\ -\mathbf{G}_{\mathrm{a}}(\beta) & \mathbf{H}_{\mathrm{a}}(\beta) & \mathbf{0} \\ \mathbf{0} & -\mathbf{C}_{\mathrm{a}} & \mathbf{K}_{\mathrm{e}}(\beta)-\omega^2\mathbf{M}_{\mathrm{e}} \end{bmatrix} \begin{bmatrix} \tilde{\mathbf{v}}_{\mathrm{an}} \\ \tilde{\mathbf{p}}_{\mathrm{a}} \\ \tilde{\mathbf{u}}_{\mathrm{e}} \end{bmatrix} = \begin{bmatrix} \mathbf{0} \\ \mathbf{0} \\ \tilde{\mathbf{F}}_{\mathrm{e}} \end{bmatrix}, \tag{11}$$

where $\mathbf{I}_{\mathrm{ae}}$ is a unit matrix; $\mathbf{E}_{\mathrm{e}}$ is a matrix formed with elements being either 0 or the components of the normal vector at the interface, used to project the nodal displacement of the solid on the direction normal to the interface. $\mathbf{C}_{\mathrm{a}}$ times $\tilde{\mathbf{p}}_{\mathrm{a}}$ gives the nodal forces applied by the external fluid to the elastic solid. The second equation in Eq. (11) is just Eq. (8).

2.2 A 2.5D FE model for a poro-elastic medium

2.2.1 Strong formulation

According to the classical Biot's theory [14][15] (with displacements as unknown functions), the differential equations of motion governing vibrations of the solid frame and fluid (two phases) in a poro-elastic medium without externally applied body force is given by

$$\begin{cases} \left(\tilde{P}-N\right)\nabla\nabla\cdot\mathbf{u}+N\nabla^2\mathbf{u}+\tilde{Q}\nabla\nabla\cdot\mathbf{U}+\omega^2\left(\tilde{\rho}_{11}\mathbf{u}+\tilde{\rho}_{12}\mathbf{U}\right)=0 \\ \tilde{R}\nabla\nabla\cdot\mathbf{U}+\tilde{Q}\nabla\nabla\cdot\mathbf{u}+\omega^2\left(\tilde{\rho}_{22}\mathbf{U}+\tilde{\rho}_{12}\mathbf{u}\right)=0 \end{cases} \tag{12}$$

where $\tilde{P}$, $\tilde{Q}$ and $\tilde{R}$ are the elastic coefficients with $\tilde{Q}$ representing the stress-strain coupling between the two phases. The tilde indicates that the associated parameter is complex and frequency dependent. The dependence of the parameters on frequency is caused by damping arising from the thermal conductivity between the two phases. $\mathbf{u}$ and $\mathbf{U}$ are, respectively, the displacement vectors of the solid frame and interstitial fluid; N is the shear modulus of the porous material; $\tilde{\rho}_{11}$, $\tilde{\rho}_{22}$ and $\tilde{\rho}_{12}$ are the mass coefficients with $\tilde{\rho}_{12}$ describing the inertial coupling between the two phases. Again, they are frequency-dependent, due to the viscous damping arising from relative motion between the solid and fluid.

A FE model for the poro-elastic medium may be generated based on Eq. (12) (strong

formulation) with each node having six degrees of freedom. As demonstrated previously [9]-[13], the FE matrices are implicitly frequency-dependent, requiring reconstruction at each frequency in a spectral analysis. This, combined with the six degrees of freedom at each node, may requires too high computational effort. Fortunately, the mixed displacement-pressure formulation of Biot's theory, based on which weak integrals can be established, can be used to overcome these disadvantages [18], as detailed below.

2.2.2 Weak formulation

According to Ref. [18], the mixed displacement-pressure formulation of Biot's theory is given by

$$\nabla \cdot \bar{\bar{\sigma}}_{ij}^{\mathrm{s}} + \omega^2 \tilde{\rho} \mathbf{u} + \tilde{\gamma} \nabla p = \mathbf{0} \tag{13}$$

$$\nabla^2 p + \frac{\omega^2 \tilde{\rho}_{22}}{\tilde{R}} p - \frac{\omega^2 \tilde{\rho}_{22}}{\phi^2} \tilde{\gamma} \nabla \cdot \mathbf{u} = 0 \tag{14}$$

where superscript s is used to indicate solid frame of a poro-elastic medium; $\bar{\bar{\sigma}}_{ij}^{\mathrm{s}}$ is the stress tensor of the solid frame in vacuum; p is the fluid in-pore pressure; ϕ is the porosity of the porous medium; $\tilde{\rho} = \tilde{\rho}_{11} - \left(\tilde{\rho}_{12}\right)^2 / \tilde{\rho}_{22}$ and $\tilde{\gamma} = \phi\left(\tilde{\rho}_{12} / \tilde{\rho}_{22} - \tilde{Q} / \tilde{R}\right)$, functions of the elastic and mass coefficients appearing in Eq. (12). The model of Johnson et al. [30] and the Champoux-Allard model [31] are used to obtain these coefficients in this work.

By integrating Eqs. (13) and (14) over the volume occupied by the poro-elastic medium and using the divergence theorem and the partial integral technique, the so-called weak integrals of the mixed displacement-pressure governing equations of Biot's theory are obtained [19]

$$\int_V \bar{\bar{\sigma}}_{ij}^{\mathrm{s}} \delta \varepsilon_{ij}^{\mathrm{s}} \mathrm{d}v - \omega^2 \int_V \tilde{\rho} \mathbf{u} \delta \mathbf{u} \mathrm{d}v - \int_V \tilde{\gamma} \nabla p \delta \mathbf{u} \mathrm{d}v - \int_\Omega \bar{\bar{\sigma}}_{ij}^{\mathrm{s}} \delta u_i n_j \mathrm{d}\Omega = 0, \tag{15}$$

$$\int_V \left(\frac{\phi^2}{\omega^2 \tilde{\rho}_{22}} \nabla p \cdot \nabla \delta p - \frac{\phi^2}{\tilde{R}} p \delta p \right) \mathrm{d}v - \int_V \tilde{\gamma} \mathbf{u} \cdot \nabla \delta p \mathrm{d}v + \int_\Omega \left(\tilde{\gamma} u_{\mathrm{n}} - \frac{\phi^2}{\omega^2 \tilde{\rho}_{22}} \frac{\partial p}{\partial \mathbf{n}} \right) \delta p \mathrm{d}\Omega = 0, \tag{16}$$

where V is denoted as the volume occupied by the medium; $\varepsilon_{ij}^{\mathrm{s}}$ is the strain tensor of the solid frame in vacuum; n_j is the jth component of the unit normal vector $\mathbf{n}$ on the boundary (denoted by Ω), pointing out of the poro-elastic medium; u_{n} is the normal displacement of the frame on the boundary. Eqs. (15) and (16) will be used to generate the 2.5D FE models of the solid frame and the

interstitial fluid.

2.2.3 2.5D FE modelling

Since the poro-elasic medium is assumed to be uniform in the *x*-direction, the three-dimensional response at any cross-section can be interpolated with the same shape functions based on the same 2D FE mesh. In other words, it can be written out that

$$\begin{cases} \mathbf{u}(x,y,z) = \mathbf{N}_{\mathrm{s}}(y,z)\bar{\mathbf{u}}(x,y,z) \\ p(x,y,z) = \mathbf{N}_{\mathrm{f}}(y,z)\bar{\mathbf{p}}(x,y,z) \end{cases}, \tag{17}$$

where the subscript f is used to indicate the interstitial fluid in a poro-elastic medium; $\bar{\mathbf{u}}(x,y,z)$ is the vector of nodal displacement amplitudes of the solid frame; $\bar{\mathbf{p}}(x,y,z)$ is the vector of nodal pressure amplitudes of the interstitial fluid; $\mathbf{N}_{\mathrm{s}}(y,z)$ and $\mathbf{N}_{\mathrm{f}}(y,z)$ are the corresponding shape function matrices.

Substituting Eq. (17) into the first three integrands in Eq. (15) gives

$$\bar{\bar{\sigma}}_{ij}^{\mathrm{s}}\delta\varepsilon_{ij}^{\mathrm{s}} = \left[\left(\mathbf{L}_0 + \frac{\partial}{\partial x}\mathbf{L}_1\right)\mathbf{N}_{\mathrm{s}}(y,z)\delta\bar{\mathbf{u}}(x,y,z)\right]^{\mathrm{H}}\mathbf{D}\left[\left(\mathbf{L}_0 + \frac{\partial}{\partial x}\mathbf{L}_1\right)\mathbf{N}_{\mathrm{s}}(y,z)\bar{\mathbf{u}}(x,y,z)\right], \tag{18}$$

$$\tilde{\rho}\mathbf{u}\delta\mathbf{u} = \tilde{\rho}\delta\bar{\mathbf{u}}(x,y,z)^{\mathrm{H}}\mathbf{N}_{\mathrm{s}}(y,z)^{\mathrm{T}}\mathbf{N}_{\mathrm{s}}(y,z)\bar{\mathbf{u}}(x,y,z), \tag{19}$$

$$\tilde{\gamma}\nabla p\delta\mathbf{u} = \tilde{\gamma}\delta\bar{\mathbf{u}}(x,y,z)^{\mathrm{H}}\mathbf{N}_{\mathrm{s}}(y,z)^{\mathrm{H}}\left(\mathbf{B}_0 + \frac{\partial}{\partial x}\mathbf{B}_1\right)\mathbf{N}_{\mathrm{f}}(y,z)\bar{\mathbf{p}}(x,y,z), \tag{20}$$

where superscripts H and T denote conjugate transpose and transpose, respectively; $\mathbf{D}$ is the stress-strain matrix of the solid frame; $\left(\mathbf{L}_0 + \frac{\partial}{\partial x}\mathbf{L}_1\right)$ is the strain-displacement matrix of the solid frame; $\left(\mathbf{B}_0 + \frac{\partial}{\partial x}\mathbf{B}_1\right)$ is the gradient operator ∇.

Then, substitution of Eqs. (18), (19) and (20) into Eq. (15) yields

$$\int_x \left(\sum_{i=0}^{1}\sum_{j=0}^{1}\frac{\partial^i\delta\bar{\mathbf{u}}^{\mathrm{H}}}{\partial x^i}\mathbf{A}_{ij}\frac{\partial^j\bar{\mathbf{u}}}{\partial x^j} - \omega^2\delta\bar{\mathbf{u}}^{\mathrm{H}}\mathbf{M}_{\mathrm{s}}\bar{\mathbf{u}} - \sum_{j=0}^{1}\delta\bar{\mathbf{u}}^{\mathrm{H}}\mathbf{C}_j\frac{\partial^j\bar{\mathbf{p}}}{\partial x^j}\right)\mathrm{d}x = \int_\Omega \bar{\bar{\sigma}}_{ij}^{\mathrm{s}}\delta u_i n_j \mathrm{d}\Omega, \tag{21}$$

where

$$\begin{cases} \mathbf{A}_{ij} = \int_A \left(\mathbf{L}_i \mathbf{N}_\mathrm{s}\right)^\mathrm{T} \mathbf{D} \mathbf{L}_j \mathbf{N}_\mathrm{s} \mathrm{d}A \\ \mathbf{M}_\mathrm{s} = \int_A \tilde{\rho} \mathbf{N}_\mathrm{s}^\mathrm{T} \mathbf{N}_\mathrm{s} \mathrm{d}A \\ \mathbf{C}_{sj} = \int_A \tilde{\gamma} \mathbf{N}_\mathrm{s}^\mathrm{T} \mathbf{B}_j \mathbf{N}_\mathrm{f} \mathrm{d}A \end{cases}, \tag{22}$$

where A is the area of the cross-section. From Eq. (22) it can be seen that, since for a given poro-elastic medium $\tilde{\rho}$ and $\tilde{\gamma}$ are space-invariant, the integrals for matrices $\mathbf{M}_\mathrm{s}$ and $\mathbf{C}_{sj}$ do not have to be calculated for every frequency but instead, they can be calculated once without the presence of $\tilde{\rho}$ and $\tilde{\gamma}$, with the results multiplied by $\tilde{\rho}$ and $\tilde{\gamma}$ to give matrices $\mathbf{M}_\mathrm{s}$ and $\mathbf{C}_{sj}$ at every frequency.

Since the poro-elastic medium is assumed to be infinitely long in the x-direction, the solid displacement and fluid pressure can be expressed as superposition of waves propagating in the x-direction at particular wavenumbers, as shown in Eq. (3). Therefore, at a given wavenumber β, $\bar{\mathbf{u}}\left(x, y, z\right)$ and $\bar{\mathbf{p}}\left(x, y, z\right)$ can be expressed as

$$\begin{cases} \bar{\mathbf{u}}\left(x, y, z\right) = \tilde{\mathbf{u}}_\mathrm{s}\left(y, z\right) \mathrm{e}^{-\mathrm{i}\beta x} \\ \bar{\mathbf{p}}\left(x, y, z\right) = \tilde{\mathbf{p}}_\mathrm{f}\left(y, z\right) \mathrm{e}^{-\mathrm{i}\beta x} \end{cases}, \tag{23}$$

where $\tilde{\mathbf{u}}_\mathrm{s}\left(y, z\right)$ is the vector of nodal displacement amplitudes of the solid frame on the cross-section; $\tilde{\mathbf{p}}_\mathrm{f}\left(y, z\right)$ is the corresponding vector of nodal pressure amplitudes of the interstitial fluid.

By substituting Eqs. (23) into (21), it yields

$$\delta\tilde{\mathbf{u}}_\mathrm{s}^\mathrm{H} \left[\left(-\mathrm{i}\beta\right)^2 \mathbf{K}_{\mathrm{s}2} + \left(-\mathrm{i}\beta\right) \mathbf{K}_{\mathrm{s}1} + \mathbf{K}_{\mathrm{s}0} - \omega^2 \mathbf{M}_\mathrm{s} \quad -\mathbf{C}_{\mathrm{s}0} - \left(-\mathrm{i}\beta\right) \mathbf{C}_{\mathrm{s}1} \right] \left(\tilde{\mathbf{u}}_\mathrm{s}^\mathrm{T} \quad \tilde{\mathbf{p}}_\mathrm{f}^\mathrm{T} \right)^\mathrm{T} = \delta\tilde{\mathbf{u}}_\mathrm{s}^\mathrm{H} \tilde{\mathbf{F}}_\mathrm{s}, \tag{24}$$

where $\tilde{\mathbf{F}}_\mathrm{s}$ represents the vector of equivalent nodal force amplitudes on the boundary applied to the solid frame; $\mathbf{K}_{\mathrm{s}2} = -\mathbf{A}_{11}$, $\mathbf{K}_{\mathrm{s}1} = \mathbf{A}_{01} - \mathbf{A}_{10}$ and $\mathbf{K}_{\mathrm{s}0} = \mathbf{A}_{00}$.

The same procedure is applied to Eq. (16) for the interstitial fluid, giving

$$\delta\tilde{\mathbf{p}}_\mathrm{f}^\mathrm{H} \left[\frac{1}{\omega^2} \left(\left(-\mathrm{i}\beta\right)^2 \mathbf{K}_{\mathrm{f}2} + \left(-\mathrm{i}\beta\right) \mathbf{K}_{\mathrm{f}1} + \mathbf{K}_{\mathrm{f}0} \right) - \mathbf{M}_\mathrm{f} \quad -\mathbf{C}_{\mathrm{f}0} + \left(-\mathrm{i}\beta\right) \mathbf{C}_{\mathrm{f}1} \right] \left(\tilde{\mathbf{p}}_\mathrm{f}^\mathrm{T} \quad \tilde{\mathbf{u}}_\mathrm{s}^\mathrm{T} \right)^\mathrm{T} = \delta\tilde{\mathbf{p}}_\mathrm{f}^\mathrm{H} \tilde{\mathbf{F}}_\mathrm{f}, \tag{25}$$

where $\tilde{\mathbf{F}}_\mathrm{f}$ represents the vector of generalized nodal force amplitudes on the boundary applied to the interstitial fluid; $\mathbf{K}_{\mathrm{f}2} = -\mathbf{R}_{11}$, $\mathbf{K}_{\mathrm{f}1} = \mathbf{R}_{01} - \mathbf{R}_{10} = \mathbf{0}$, $\mathbf{K}_{\mathrm{f}0} = \mathbf{R}_{00}$ and

$$\begin{cases} \mathbf{R}_{ij} = \int_A \dfrac{\phi^2}{\tilde{\rho}_{22}} \left(\mathbf{B}_i \mathbf{N}_{\mathrm{f}}\right)^{\mathrm{T}} \mathbf{B}_j \mathbf{N}_{\mathrm{f}} \mathrm{d}A \\ \mathbf{M}_{\mathrm{f}} = \int_A \dfrac{\phi^2}{\tilde{R}} \mathbf{N}_{\mathrm{f}}^{\mathrm{T}} \mathbf{N}_{\mathrm{f}} \mathrm{d}A \\ \mathbf{C}_{\mathrm{f}j} = \int_A \tilde{\gamma} \left(\mathbf{B}_j \mathbf{N}_{\mathrm{f}}\right)^{\mathrm{T}} \mathbf{N}_{\mathrm{s}} \mathrm{d}A \end{cases} . \tag{26}$$

It can be seen from Eqs. (22) and (26) that $\mathbf{C}_{sj} = \mathbf{C}_{\mathrm{f}j}^{\mathrm{T}}$. Similar to the calculation of matrices $\mathbf{M}_{\mathrm{s}}$ and $\mathbf{C}_{sj}$ in Eq. (22), the integrals for matrices $\mathbf{R}_{ij}$, $\mathbf{M}_{\mathrm{f}}$ and $\mathbf{C}_{\mathrm{f}j}$ in Eq. (26) can be calculated once without the presence of the frequency-dependant material parameters, with the results multiplied by those parameters o give the matrices at every frequency.

By combining Eq. (24) with Eq. (25) and considering the arbitrariness of the admissible or virtual displacement and pressure, a 2.5D FE equation (model) for the poro-elastic medium is yielded

$$\begin{bmatrix} \mathbf{K}_{\mathrm{s}}(\beta) - \omega^2 \mathbf{M}_{\mathrm{s}} & \mathbf{C}_{\mathrm{s}} \\ \mathbf{C}_{\mathrm{f}} & \dfrac{1}{\omega^2} \mathbf{K}_{\mathrm{f}}(\beta) - \mathbf{M}_{\mathrm{f}} \end{bmatrix} \begin{pmatrix} \tilde{\mathbf{u}}_{\mathrm{s}} \\ \tilde{\mathbf{p}}_{\mathrm{f}} \end{pmatrix} = \begin{pmatrix} \tilde{\mathbf{F}}_{\mathrm{s}} \\ \tilde{\mathbf{F}}_{\mathrm{f}} \end{pmatrix}, \tag{27}$$

where

$$\begin{cases} \mathbf{K}_{\mathrm{s}} = \left(-\mathrm{i}\beta\right)^2 \mathbf{K}_{\mathrm{s}2} + \left(-\mathrm{i}\beta\right) \mathbf{K}_{\mathrm{s}1} + \mathbf{K}_{\mathrm{s}0} \\ \mathbf{C}_{\mathrm{s}} = -\mathbf{C}_{\mathrm{s}0} - \left(-\mathrm{i}\beta\right) \mathbf{C}_{\mathrm{s}1} \\ \mathbf{K}_{\mathrm{f}} = \left(-\mathrm{i}\beta\right)^2 \mathbf{K}_{\mathrm{f}2} + \mathbf{K}_{\mathrm{f}0} \\ \mathbf{C}_{\mathrm{f}} = -\mathbf{C}_{\mathrm{f}0} + \left(-\mathrm{i}\beta\right) \mathbf{C}_{\mathrm{f}1} \end{cases}, \tag{28}$$

It can be found from Eqs. (28) that $\mathbf{C}_{\mathrm{s}} = \mathbf{C}_{\mathrm{f}}^{\mathrm{H}}$.

The 2.5D FE model of the poro-elastic medium may need to be coupled with those of solids, internal fluids and other poro-elastic media in the structure, as well as with the 2.5D BE models of the external acoustic fluids on both sides of the structure. These couplings are discussed in the next section.

2.3 Coupling of poro-elastic media with other media

Together with the boundary conditions described in Refs. [10][20], the last boundary integral in Eq. (15)

$$I_1 = -\int_\Omega \bar{\bar{\sigma}}_{ij}^{\mathrm{s}} \delta u_i n_j \mathrm{d}\Omega, \tag{29}$$

and the last boundary integral in Eq. (16)

$$I_2 = \int_\Omega \left(\tilde{\gamma} u_{\mathrm{n}} - \frac{\phi^2}{\omega^2 \tilde{\rho}_{22}} \frac{\partial p}{\partial \mathbf{n}} \right) \delta p \mathrm{d}\Omega, \tag{30}$$

will be used to perform the coupling of a poro-elastic medium with another poro-elastic medium, a solid, or a fluid.

2.3.1 Coupling between two poro-elastic media

Suppose two poro-elastic media are physically coupled at a common interface. Let indices 1 and 2 denote the associated variables for the porous media. The boundary integrals in Eqs. (29) and (30) for porous medium 1 are denoted by I_1^1 and I_2^1, and those for the second porous medium by I_1^2 and I_2^2. According to Refs [10][20], the boundary conditions at the interface, of which the normal $\mathbf{n} = (n_1, n_2, n_3)$ points out of porous medium 1, are given by

$$\begin{cases} \sigma_{ij,1}^{\mathrm{t}} n_j = \sigma_{ij,2}^{\mathrm{t}} n_j \\ \phi_1 \left(U_{i,1} - u_{i,1} \right) n_i = \phi_2 \left(U_{i,2} - u_{i,2} \right) n_i \\ u_{i,1} = u_{i,2} \\ p_1 = p_2 \end{cases}, \tag{31}$$

where σ_{ij}^{t} is the total stress tensor combining the contributions of the solid frame and the interstitial fluid; U_i is the *i*th displacement component of the interstitial fluid. The first equation ensures the continuity of total normal stress at the interface; the second equation ensures the continuity of relative mass flux across the interface; the last two equations ensure the continuity of solid frame displacement and fluid in-pore pressure at the interface. By substituting Eq. (31) into $I_1^1 + I_1^2$ and $I_2^1 + I_2^2$, the coupling between the two porous media can be enforced by

$$\begin{cases} I_1^1 + I_1^2 = -\int_\Omega \phi_1 \left(1 + \dfrac{\tilde{Q}_1}{\tilde{R}_1} \right) p_1 n_i \delta u_{i,1} \mathrm{d}\Omega + \int_\Omega \phi_2 \left(1 + \dfrac{\tilde{Q}_2}{\tilde{R}_2} \right) p_2 n_i \delta u_{i,2} \mathrm{d}\Omega \\ I_2^1 + I_2^2 = -\int_\Omega \phi_1 \left(1 + \dfrac{\tilde{Q}_1}{\tilde{R}_1} \right) u_{i,1} n_i \delta p_1 d\Omega + \int_\Omega \phi_2 \left(1 + \dfrac{\tilde{Q}_2}{\tilde{R}_2} \right) u_{i,2} n_i \delta p_2 d\Omega \\ u_{i,1} = u_{i,2} \\ p_1 = p_2 \end{cases}, \tag{32}$$

where the last two equations should be explicitly applied at the interface; $\tilde{Q}_1$, $\tilde{Q}_2$, $\tilde{R}_1$ and $\tilde{R}_2$ are

the frequency-dependent elastic constants of the solid frames of the two poro-elastic media.

With a mesh at the interface, the first two equations in Eq. (32) can be rewritten as

$$I_1^1 + I_1^2 = -\int_\Omega \phi_1 \left(1+\frac{\tilde{Q}_1}{\tilde{R}_1}\right) \delta\tilde{\mathbf{u}}_{s1}'^{\mathrm{H}} \mathbf{N}_{s1}'^{\mathrm{T}} \mathbf{n}^{\mathrm{T}} \mathbf{N}_{f1}' \tilde{\mathbf{p}}_{f1}' \mathrm{d}\Omega + \int_\Omega \phi_2 \left(1+\frac{\tilde{Q}_2}{\tilde{R}_2}\right) \delta\tilde{\mathbf{u}}_{s2}'^{\mathrm{H}} \mathbf{N}_{s2}'^{\mathrm{T}} \mathbf{n}^{\mathrm{T}} \mathbf{N}_{f2}' \tilde{\mathbf{p}}_{f2}' \mathrm{d}\Omega, \tag{33}$$

$$I_2^1 + I_2^2 = -\int_\Omega \phi_1 \left(1+\frac{\tilde{Q}_1}{\tilde{R}_1}\right) \delta\tilde{\mathbf{p}}_{f1}'^{\mathrm{H}} \mathbf{N}_{f1}'^{\mathrm{T}} \mathbf{n} \mathbf{N}_{s1}' \tilde{\mathbf{u}}_{s1}' \mathrm{d}\Omega + \int_\Omega \phi_2 \left(1+\frac{\tilde{Q}_2}{\tilde{R}_2}\right) \delta\tilde{\mathbf{p}}_{f2}'^{\mathrm{H}} \mathbf{N}_{f2}'^{\mathrm{T}} \mathbf{n} \mathbf{N}_{s2}' \tilde{\mathbf{u}}_{s2}' \mathrm{d}\Omega, \tag{34}$$

where $\tilde{\mathbf{u}}_{s1}'$ and $\tilde{\mathbf{u}}_{s2}'$ are the vectors of nodal displacement amplitudes of the solid frames of the two porous media at the interface; $\tilde{\mathbf{p}}_{f1}'$ and $\tilde{\mathbf{p}}_{f2}'$ are the corresponding vectors of nodal pressure amplitudes; $\mathbf{N}_{s1}'$ and $\mathbf{N}_{f1}'$ are the shape function matrices for the solid displacement and fluid pressure at the interface of porous medium 1, and $\mathbf{N}_{s2}'$ and $\mathbf{N}_{f2}'$ are the corresponding matrices for porous medium 2.

By combining Eqs. (33) and (34) with the 2.5D FE models of the two porous media, i.e. Eq. (27) and imposing the third and fourth equations of Eq. (32) by using a Lagrange multiplier, the 2.5D FE model governing vibration of the two porous media yields

$$\begin{bmatrix}
\mathbf{K}_{s1}-\omega^2\mathbf{M}_{s1} & \mathbf{C}_{s1}+\mathbf{I}_{s1} & \mathbf{0} & \mathbf{0} & \mathbf{A}_{s1}^{\mathrm{T}} & \mathbf{0} \\
\mathbf{C}_{f1}+\mathbf{I}_{f1} & \frac{1}{\omega^2}\mathbf{K}_{f1}-\mathbf{M}_{f1} & \mathbf{0} & \mathbf{0} & \mathbf{0} & \mathbf{A}_{f1}^{\mathrm{T}} \\
\mathbf{0} & \mathbf{0} & \mathbf{K}_{s2}-\omega^2\mathbf{M}_{s2} & \mathbf{C}_{s2}+\mathbf{I}_{s2} & -\mathbf{A}_{s2}^{\mathrm{T}} & \mathbf{0} \\
\mathbf{0} & \mathbf{0} & \mathbf{C}_{f2}+\mathbf{I}_{f2} & \frac{1}{\omega^2}\mathbf{K}_{f2}-\mathbf{M}_{f2} & \mathbf{0} & -\mathbf{A}_{f2}^{\mathrm{T}} \\
\mathbf{A}_{s1} & \mathbf{0} & -\mathbf{A}_{s2} & \mathbf{0} & \mathbf{0} & \mathbf{0} \\
\mathbf{0} & \mathbf{A}_{f1} & \mathbf{0} & -\mathbf{A}_{f2} & \mathbf{0} & \mathbf{0}
\end{bmatrix}
\begin{bmatrix}
\tilde{\mathbf{u}}_{s1} \\ \tilde{\mathbf{p}}_{f1} \\ \tilde{\mathbf{u}}_{s2} \\ \tilde{\mathbf{p}}_{f2} \\ \tilde{\boldsymbol{\lambda}}_{s(1,2)} \\ \tilde{\boldsymbol{\lambda}}_{f(1,2)}
\end{bmatrix}
=
\begin{bmatrix}
\tilde{\mathbf{F}}_{s1} \\ \tilde{\mathbf{F}}_{f1} \\ \tilde{\mathbf{F}}_{s2} \\ \tilde{\mathbf{F}}_{f2} \\ \tilde{\mathbf{F}}_{\lambda s(1,2)} \\ \tilde{\mathbf{F}}_{\lambda f(1,2)}
\end{bmatrix} \tag{35}$$

where $\tilde{\boldsymbol{\lambda}}_{s(1,2)}$ and $\tilde{\boldsymbol{\lambda}}_{f(1,2)}$ are the Lagrange multiplier vectors, and $\tilde{\mathbf{F}}_{\lambda s(1,2)}$ and $\tilde{\mathbf{F}}_{\lambda f(1,2)}$ are the associated vectors of nodal force amplitudes. $\mathbf{A}_{s1}$ and $\mathbf{A}_{f1}$ contain elements of 0 and 1, transforming the nodal displacements of the solid frame and the nodal pressure of the interstitial fluid to those at the interface of porous medium 1; $\mathbf{A}_{s2}$ and $\mathbf{A}_{f2}$ are the similar matrices of porous medium 2;

$$\mathbf{I}_{s1} = -\int_\Omega \phi_1 \left(1+\frac{\tilde{Q}_1}{\tilde{R}_1}\right) \mathbf{N}_{s1}'^{\mathrm{T}} \mathbf{n}^{\mathrm{T}} \mathbf{N}_{f1}' \mathrm{d}\Omega; \tag{36}$$

$$\mathbf{I}_{s2}=\int_{\Omega}\phi_2\left(1+\frac{\tilde{Q}_2}{\tilde{R}_2}\right)\mathbf{N}_{s2}'^{\mathrm{T}}\mathbf{n}^{\mathrm{T}}\mathbf{N}_{f2}'\mathrm{d}\Omega\,; \tag{37}$$

$$\mathbf{I}_{f1}=-\int_{\Omega}\phi_1\left(1+\frac{\tilde{Q}_1}{\tilde{R}_1}\right)\mathbf{N}_{f1}'^{\mathrm{T}}\mathbf{n}\mathbf{N}_{s1}'\mathrm{d}\Omega\,; \tag{38}$$

$$\mathbf{I}_{f2}=\int_{\Omega}\phi_2\left(1+\frac{\tilde{Q}_2}{\tilde{R}_2}\right)\mathbf{N}_{f2}'^{\mathrm{T}}\mathbf{n}\mathbf{N}_{s2}'\mathrm{d}\Omega\,. \tag{39}$$

It can be found from Eqs. (36), (37), (38) and (39) that $\mathbf{I}_{s1}=\mathbf{I}_{f1}^{\mathrm{T}}$ and $\mathbf{I}_{s2}=\mathbf{I}_{f2}^{\mathrm{T}}$.

2.3.2 Coupling between a poro-elastic medium and a solid

A similar procedure is used to establish the coupling between a poro-elastic medium and a solid domain. Let subscript or superscript ‘e’ denote the associated variables of elastic solids in the structure. The boundary conditions at the interface of a poro-elastic medium with an elastic solid are given by Refs. [10][20] as

$$\begin{cases}\sigma_{ij}^{\mathrm{t}}n_j=\sigma_{ij}^{\mathrm{e}}n_j\\ U_in_i=u_in_i\\ u_i=u_i^{\mathrm{e}}\end{cases}, \tag{40}$$

where the normal points out of the poro-elastic medium. The first equation represents the continuity of the total normal stress at the interface; the second equation ensures no relative mass flux across the interface; the last equation expresses the displacement continuity of the solid frame and the elastic solid at the interface.

The boundary integral for the elastic solid is given by

$$I^{\mathrm{e}}=\int_{\Omega}\sigma_{ij}^{\mathrm{e}}n_j\delta u_i^{\mathrm{e}}d\Omega\,. \tag{41}$$

Combination of Eq. (41) and Eq. (29) gives

$$I_1+I^{\mathrm{e}}=-\int_{\Omega}\sigma_{ij}^{\mathrm{t}}n_j\delta u_i d\Omega-\int_{\Omega}\phi\left(1+\frac{\tilde{Q}}{\tilde{R}}\right)pn_i\delta u_i d\Omega+\int_{\Omega}\sigma_{ij}^{\mathrm{e}}n_j\delta u_i^{\mathrm{e}}d\Omega\,. \tag{42}$$

By substituting Eq. (40) into Eqs. (30) and (42), the coupling of the poro-elastic medium with the elastic solid can be enforced by

$$\begin{cases} I_1 + I^{\mathrm{e}} = -\int_\Omega \phi \left(1 + \dfrac{\tilde{Q}}{\tilde{R}}\right) p n_i \delta u_i d\Omega \\ I_2 = -\int_\Omega \phi \left(1 + \dfrac{\tilde{Q}}{\tilde{R}}\right) u_i n_i \delta p d\Omega \\ u_i = u_i^{\mathrm{e}} \end{cases}, \tag{43}$$

where the last equation should be explicitly applied at the interface.

Similar to the derivation procedure in Section 2.3.1, combination of the 2.5D FE model of the poro-elastic medium, i.e. Eq. (27), the 2.5D FE model of the elastic solid, i.e. Eq. (4), and Eq. (43) with a 1D mesh at the interface, gives the 2.5D FE model governing vibration of the poro-elastic medium and the elastic solid as

$$\begin{bmatrix} \mathbf{K}_{\mathrm{e}} - \omega^2 \mathbf{M}_{\mathrm{e}} & \mathbf{0} & \mathbf{0} & \mathbf{A}_{\mathrm{e}}^{\mathrm{T}} \\ \mathbf{0} & \mathbf{K}_{\mathrm{s}} - \omega^2 \mathbf{M}_{\mathrm{s}} & \mathbf{C}_{\mathrm{s}} + \mathbf{I}_{\mathrm{e1}} & -\mathbf{A}_{\mathrm{s}}^{\mathrm{T}} \\ \mathbf{0} & \mathbf{C}_{\mathrm{f}} + \mathbf{I}_{\mathrm{e2}} & \dfrac{1}{\omega^2}\mathbf{K}_{\mathrm{f}} - \mathbf{M}_{\mathrm{f}} & \mathbf{0} \\ \mathbf{A}_{\mathrm{e}} & -\mathbf{A}_{\mathrm{s}} & \mathbf{0} & \mathbf{0} \end{bmatrix} \begin{bmatrix} \tilde{\mathbf{u}}_{\mathrm{e}} \\ \tilde{\mathbf{u}}_{\mathrm{s}} \\ \tilde{\mathbf{p}}_{\mathrm{f}} \\ \tilde{\boldsymbol{\lambda}} \end{bmatrix} = \begin{bmatrix} \tilde{\mathbf{F}}_{\mathrm{e}} \\ \tilde{\mathbf{F}}_{\mathrm{s}} \\ \tilde{\mathbf{F}}_{\mathrm{f}} \\ \tilde{\mathbf{F}}_{\lambda} \end{bmatrix}, \tag{44}$$

where $\tilde{\boldsymbol{\lambda}}$ is the Lagrange multiplier vector, used to apply the displacement continuity of the solid frame and the elastic solid at the interface, i.e. the third equation of Eq. (43); $\tilde{\mathbf{F}}_{\lambda}$ is the corresponding nodal force amplitude vector; $\mathbf{A}_{\mathrm{e}}$ and $\mathbf{A}_{\mathrm{s}}$ contain elements of 0 and 1, transforming the nodal displacements of the solid frame and the elastic solid to those at the interface;

$$\mathbf{I}_{\mathrm{e1}} = -\int_\Omega \phi \left(1 + \frac{\tilde{Q}}{\tilde{R}}\right) \mathbf{N}_{\mathrm{s}}'^{\mathrm{T}} \mathbf{n}^{\mathrm{T}} \mathbf{N}_{\mathrm{f}}' \mathrm{d}\Omega; \tag{45}$$

$$\mathbf{I}_{\mathrm{e2}} = -\int_\Omega \phi \left(1 + \frac{\tilde{Q}}{\tilde{R}}\right) \mathbf{N}_{\mathrm{f}}'^{\mathrm{T}} \mathbf{n} \mathbf{N}_{\mathrm{s}}' \mathrm{d}\Omega. \tag{46}$$

It can be seen from Eqs. (45) and (46) that $\mathbf{I}_{\mathrm{e1}} = \mathbf{I}_{\mathrm{e2}}^{\mathrm{T}}$.

2.3.3 Coupling between a poro-elastic medium and a fluid

Again a similar procedure is used to couple a poro-elastic medium with a fluid domain. Let subscript or superscript ‘a’ denote the associated variables of the internal fluids within the structure and the external acoustic domains on both sides of the structure. The boundary conditions at the interface are given in Refs. [10][20] as

$$\begin{cases} \sigma_{ij}^{\mathrm{t}} n_j = -p^{\mathrm{a}} \delta_{ij} n_j \\ \dfrac{1}{\rho_0 \omega^2} \dfrac{\partial p^{\mathrm{a}}}{\partial \mathbf{n}} = (1-\phi) u_i n_i + \phi U_i n_i = u_i n_i + \phi (U_i n_i - u_i n_i), \\ p = p^{\mathrm{a}} \end{cases} \tag{47}$$

where p^{a} is the pressure of the fluid and $\mathbf{n}$ is the normal (a unit vector) to the interface, pointing out of the poro-elastic medium. The first equation ensures the continuity of total normal stress at the interface; the second equation means that the relative mass flux across the interface is continuous; the third equation expresses the continuity of fluid pressure at the interface.

The boundary integral of a fluid domain is expressed as

$$I^{\mathrm{a}} = \int_{\Omega} \frac{1}{\rho_{\mathrm{a}} \omega^2} \frac{\partial p^{\mathrm{a}}}{\partial \mathbf{n}} \delta p^{\mathrm{a}} \mathrm{d}\Omega, \tag{48}$$

Combination of Eq. (48) and Eq. (30) gives

$$I_2 + I^{\mathrm{a}} = -\int_{\Omega} \phi \left(1 + \frac{\tilde{Q}}{\tilde{R}}\right) u_i n_i \delta p d\Omega - \int_{\Omega} \phi (U_i - u_i) n_i \delta p d\Omega + \int_{\Omega} \frac{1}{\rho_0 \omega^2} \frac{\partial p^{\mathrm{a}}}{\partial \mathbf{n}} \delta p^{\mathrm{a}} d\Omega. \tag{49}$$

By substituting Eq. (47) into Eqs. (29) and (49), the coupling of the poro-elastic medium with the fluid can be implemented by

$$\begin{cases} I_1 = \int_{\Omega} \left[1 - \phi \left(1 + \dfrac{\tilde{Q}}{\tilde{R}}\right)\right] p^{\mathrm{a}} n_i \delta u_i d\Omega \\ I_2 + I^{\mathrm{a}} = \int_{\Omega} \left[1 - \phi \left(1 + \dfrac{\tilde{Q}}{\tilde{R}}\right)\right] u_i n_i \delta p^{\mathrm{a}} d\Omega \\ p = p^{\mathrm{a}} \end{cases}, \tag{50}$$

where the last equation should be explicitly applied at the interface.

Similar to the derivation procedure in Section 2.3.1, combination of the 2.5D FE model of the poro-elastic medium given by Eq. (27), the 2.5D FE model of the internal fluid given by Eq. (6) and Eq. (50) with a 1D mesh at the interface, gives the 2.5D FE model governing vibration of the poro-elastic medium and the internal fluid as

$$\begin{bmatrix} \dfrac{1}{\omega^2}\mathbf{K}_{\mathrm{a}} - \mathbf{M}_{\mathrm{a}} & \mathbf{0} & \mathbf{0} & \mathbf{A}_{\mathrm{a}}^{\mathrm{T}} \\ \mathbf{0} & \mathbf{K}_{\mathrm{s}} - \omega^2 \mathbf{M}_{\mathrm{s}} & \mathbf{C}_{\mathrm{s}} + \mathbf{I}_{\mathrm{a}1} & \mathbf{0} \\ \mathbf{0} & \mathbf{C}_{\mathrm{f}} + \mathbf{I}_{\mathrm{a}2} & \dfrac{1}{\omega^2}\mathbf{K}_{\mathrm{f}} - \mathbf{M}_{\mathrm{f}} & -\mathbf{A}_{\mathrm{f}}^{\mathrm{T}} \\ \mathbf{A}_{\mathrm{a}} & \mathbf{0} & -\mathbf{A}_{\mathrm{f}} & \mathbf{0} \end{bmatrix} \begin{bmatrix} \tilde{\mathbf{p}}_{\mathrm{a}} \\ \tilde{\mathbf{u}}_{\mathrm{s}} \\ \tilde{\mathbf{p}}_{\mathrm{f}} \\ \tilde{\boldsymbol{\lambda}} \end{bmatrix} = \begin{bmatrix} \tilde{\mathbf{F}}_{\mathrm{a}} \\ \tilde{\mathbf{F}}_{\mathrm{s}} \\ \tilde{\mathbf{F}}_{\mathrm{f}} \\ \tilde{\mathbf{F}}_{\lambda} \end{bmatrix} \tag{51}$$

where $\tilde{\boldsymbol{\lambda}}$ is the Lagrange multiplier vector, used to apply the pressure continuity at the interface, i.e. the third equation of Eq. (50); $\tilde{\mathbf{F}}_{\lambda}$ is the corresponding nodal force amplitude vector; $\mathbf{A}_{\mathrm{a}}$ and $\mathbf{A}_{\mathrm{f}}$ contain elements of 0 and 1, transforming the nodal pressure of the internal fluid and the interstitial fluid in the porous medium to those at the interface;

$$\mathbf{I}_{\mathrm{a1}}=\int_{\Omega}\left[1-\phi\left(1+\frac{\tilde{Q}}{\tilde{R}}\right)\right]\mathbf{N}_{\mathrm{s}}'^{\mathrm{T}}\mathbf{n}^{\mathrm{T}}\mathbf{N}_{\mathrm{f}}'\mathrm{d}\Omega; \tag{52}$$

$$\mathbf{I}_{\mathrm{a2}}=\int_{\Omega}\left[1-\phi\left(1+\frac{\tilde{Q}}{\tilde{R}}\right)\right]\mathbf{N}_{\mathrm{f}}'^{\mathrm{T}}\mathbf{n}\mathbf{N}_{\mathrm{s}}'\mathrm{d}\Omega. \tag{53}$$

It can be seen from Eqs. (52) and (53) that $\mathbf{I}_{\mathrm{a1}}=\mathbf{I}_{\mathrm{a2}}^{\mathrm{T}}$.

For the coupling with the 2.5D BE model for the exterior acoustic domains on either side of the structure, given by Eq. (8), Eq. (51) reduces to

$$\begin{bmatrix}-\mathbf{G}_{\mathrm{a}} & \mathbf{H}_{\mathrm{a}} & \mathbf{0} & \mathbf{0}\\ \mathbf{0} & \mathbf{0} & \mathbf{K}_{\mathrm{s}}-\omega^{2}\mathbf{M}_{\mathrm{s}} & \mathbf{C}_{\mathrm{s}}+\mathbf{I}_{\mathrm{a1}}\\ -\mathbf{C}_{\mathrm{d}} & \mathbf{0} & \mathbf{C}_{\mathrm{f}}+\mathbf{I}_{\mathrm{a2}} & \frac{1}{\omega^{2}}\mathbf{K}_{\mathrm{f}}-\mathbf{M}_{\mathrm{f}}\\ \mathbf{0} & \mathbf{I}_{\mathrm{a}} & \mathbf{0} & -\mathbf{I}_{\mathrm{f}}\end{bmatrix}\begin{bmatrix}\tilde{\mathbf{v}}_{\mathrm{an}}\\ \tilde{\mathbf{p}}_{\mathrm{a}}\\ \tilde{\mathbf{u}}_{\mathrm{s}}\\ \tilde{\mathbf{p}}_{\mathrm{f}}\end{bmatrix}=\begin{bmatrix}\mathbf{0}\\ \tilde{\mathbf{F}}_{\mathrm{s}}\\ \tilde{\mathbf{F}}_{\mathrm{f}}\\ \mathbf{0}\end{bmatrix}, \tag{54}$$

where matrices $\mathbf{I}_{\mathrm{a}}$ and $\mathbf{I}_{\mathrm{f}}$ contain elements of 0 and 1, transforming the nodal pressure of the exterior fluid and the interstitial fluid to those at the interface, and are used to ensure the fluid pressure continuity at the interface; $\mathbf{C}_{\mathrm{d}}$ is used to subtract the virtual work that would otherwise be counted twice due to the implementation of the 2.5D BE method [27].

2.4 The global 2.5D FE-BE model

Having performed the couplings detailed above, a global 2.5D FE-BE vibro-acoustic model for the panel is produced, given by

$$\mathbf{D}_{\mathrm{g}}\tilde{\mathbf{V}}_{\mathrm{g}}=\tilde{\mathbf{F}}_{\mathrm{g}}, \tag{55}$$

where $\mathbf{D}_{\mathrm{g}}$ denotes the global coefficient matrix; $\tilde{\mathbf{V}}_{\mathrm{g}}$ is a vector containing the nodal displacement and pressure amplitudes in all the media, including the Lagrange multipliers for the explicit coupling of two media; $\tilde{\mathbf{F}}_{\mathrm{g}}$ is the vector of nodal force amplitudes corresponding to $\tilde{\mathbf{V}}_{\mathrm{g}}$. The 2.5D FE-BE model will be applied in Section 3 to simple multi-layered structures, serving to validate the

formulations described in Section 2.3 and the associated program. It is then applied to investigate the STL of a typical railway vehicle structure in Section 4.

2.5 Radiated sound power and STL

The vectors of nodal normal velocity amplitude $\tilde{\mathbf{v}}_{\mathrm{tn}}$ and nodal pressure amplitude $\tilde{\mathbf{p}}_{\mathrm{t}}$ at the interface of acoustic domain 2 (Fig. 1) with the panel can be obtained from Eq. (55) and used to calculate the sound power radiated into acoustic domain 2 by the panel. The sound power is given by

$$W_{\mathrm{rad}} = \frac{1}{4\pi}\mathrm{Re}\int_{-\infty}^{+\infty}\int_{0}^{l_y}\tilde{p}_{\mathrm{t}}(\beta, y)\tilde{v}_{\mathrm{tn}}^{\mathrm{H}}(\beta, y)\,\mathrm{d}\,y\,\mathrm{d}\,\beta\,, \tag{56}$$

where l_y is the width of the panel, $\tilde{v}_{\mathrm{tn}}$ is the normal velocity and $\tilde{p}_{\mathrm{t}}$ is the pressure at the interface, which can be interpolated from $\tilde{\mathbf{v}}_{\mathrm{tn}}$ and $\tilde{\mathbf{p}}_{\mathrm{t}}$.

If the panel is excited by an incident plane sound wave in acoustic domain 1 (Fig. 1) and the wave is at a single wavenumber k_x in the longitudinal direction, the structural wavenumber of the panel in the longitudinal direction is the same. The incident sound power per unit length in the x-direction can be calculated as

$$W_{\mathrm{inc}} = \frac{|\overline{p}_{\mathrm{i}}|^2 l_y \cos\theta}{2\rho_1 c_1}, \tag{57}$$

where ρ_1 and c_1 are fluid density and sound speed of acoustic domain 1, and θ is the incidence angle in Fig. 1.

The sound power transmitted by the panel per unit length in the x-direction can be evaluated as

$$W_{\mathrm{trans}} = \frac{1}{2}\mathrm{Re}\int_{0}^{l_y}\tilde{p}_{\mathrm{t}}(y)\tilde{v}_{\mathrm{tn}}^{\,*}(y)\,\mathrm{d}\,y\,, \tag{58}$$

where '*' denotes the complex conjugate. The ratio of the transmitted sound power to the incident sound power gives the sound power transmission coefficient τ which is used to calculate the sound transmission loss of the panel, i.e.

$$\tau = \frac{W_{\mathrm{trans}}}{W_{\mathrm{inc}}}, \tag{59}$$

$$\mathrm{STL} = 10\log_{10}\left(\frac{1}{\tau}\right). \tag{60}$$

The diffuse field sound transmission loss can be calculated as

$$\mathrm{STL}_{\mathrm{d}} = 10\log_{10}(\frac{1}{\tau_{\mathrm{d}}}), \tag{61}$$

where τ_{d} is the diffuse field sound power transmission coefficient, given by

$$\tau_{\mathrm{d}} = \frac{\int_{\psi_{\mathrm{lim}}}^{\pi/2}\int_{\varphi_{\mathrm{lim}}}^{\pi/2}\tau(\psi,\varphi)\sin^2\psi\sin\varphi\mathrm{d}\varphi\mathrm{d}\psi}{\int_{\psi_{\mathrm{lim}}}^{\pi/2}\int_{\varphi_{\mathrm{lim}}}^{\pi/2}\sin^2\psi\sin\varphi\mathrm{d}\varphi\mathrm{d}\psi}, \tag{62}$$

where φ_{lim} and ψ_{lim} are the integral limiting angles, which are set to be 12 ºfor 'field incidence' and 0 ºfor full random incidence [25][32]. In this work, the full random incidence is considered.

3. Application to layered structures

The 2.5D FE-BE model developed in Section 2 is now applied to study the vibro-acoustic behaviours of structures layered by one solid plate and porous materials. More specifically, the following two applications are presented: 1) prediction of the surface normal impedance of a porous material layer backed by a rigid impervious wall; 2) prediction of the STL of a plate attached with layers of porous material and/or air. In each application, comparisons are made with other established methodologies.

3.1 Surface normal impedance of a single porous layer

As the first application, the surface normal impedance of a 100 mm thick layer of glass wool is calculated using the 2.5D model developed in Section 2.2 (now the model has only one poro-elastic medium and one acoustic domain (acoustic domain 1, see Fig. 1)) and compared with results in Ref. [18]. The layer of glass wool in the 2.5D FE model is infinitely long in the *x*-direction but has a width of 2 m to mimic an infinite width in the *y*-direction. The layer of glass wool is backed by a rigid impervious wall. The cross-section is meshed with 8-noded 2.5D solid elements (with quadratic interpolation). An element size of 15 mm is used in the thickness direction and 75 mm in the lateral direction. The properties of the glass wool are listed in Tab. 1 where α_∞ represents the tortuosity, ϕ is the porosity, σ is the flow resistivity, and Λ and Λ' are the viscous and thermal characteristic lengths. For the frame in vacuum, ρ_{s} represents the density, E is the Young's modulus,

v is Poisson's ratio and η is the loss factor.

Tab. 1 Properties of the melamine foam [27] and glass wool [18]

Porous material	α_∞	ϕ	σ (Ns/m^4)	Λ (μm)	Λ' (μm)	ρ_s (kg/m^3)	E (N/m^2)	v	η
Melamine foam	1.06	0.97	11000	150	200	11	1.2×10^5	0.42	0.15
Glass wool	1.06	0.94	40000	56	110	130	4.4×10^6	0	0.1

The surface normal impedance of the porous material layer is given in Ref. [18] by

$$Z_{\mathrm{n}} = \frac{1}{\mathrm{i}\omega\left[(1-\phi)u_{\mathrm{n}} + \phi U_{\mathrm{n}}\right]}, \tag{63}$$

where u_{n} is the normal displacement of the solid frame on the surface of the porous material layer receiving a unit normally incident plane wave, and U_{n} is that of the interstitial fluid. According to the mixed displacement-pressure formulation [18], U_{n} is described as

$$U_n = \left(\frac{\phi}{\tilde{\rho}_{22}\omega^2}\nabla p - \frac{\tilde{\rho}_{12}}{\tilde{\rho}_{22}}\mathbf{u}\right)\cdot\mathbf{n}, \tag{64}$$

where $\mathbf{n}$ is the unit normal vector on the surface of the glass wool, pointing out of the poro-elastic medium. Using Eq. (55), the pressure gradient ∇p and solid frame displacements $\mathbf{u}$ on the surface can be obtained.

Fig. 3 shows the real and imaginary parts of the surface normal impedance. For comparison, results predicted using the transfer matrix method (TMM) based on a poro-rigid frame model are also plotted. It can be seen that, results from the 2.5D FE-BE model agree well with those from Ref. [18]. However, there are apparent differences between the models allowing for the frame vibration and the poro-rigid TMM assuming an infinite width for the layer, when frequencies are below around 1000 Hz. In the 2.5D FE-BE prediction, the real part has a dip at around 455 Hz and the imaginary part has a peak at 478 Hz. They are due to the resonance of the solid frame, at which the compressional wavelength of the frame is equal to four times the thickness of the porous material layer [7], i.e.

$$f_{\mathrm{r}} = \frac{1}{4h}\Big/\sqrt{\frac{\rho_{\mathrm{s}}}{K_{\mathrm{c}}} - \frac{1}{c_1^2}\sin^2\theta}, \tag{65}$$

where θ is the incident angle (Fig. 1), c_1 is the sound speed of the external fluid, and

$$K_c = \frac{(1-\nu)E}{(1+\nu)(1-2\nu)}. \tag{66}$$

With the elastic parameters of the glass wool listed in Tab. 1, Eq. (65) gives 460 Hz, close to the frequencies of the dip in the real part and the peak in the imaginary part.

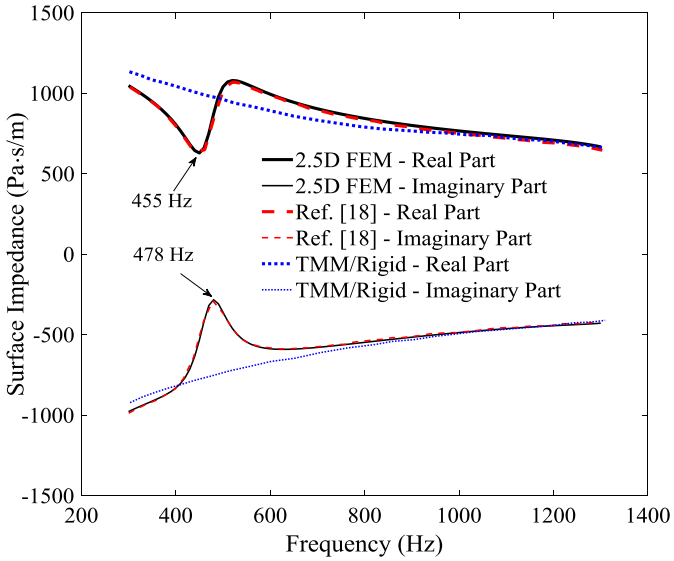

Fig. 3 Surface normal impedance predicted for a 100 mm thick glass wool layer backed by a rigid impervious wall

3.2 STL of a panel laminated with a plate, porous material layers and/or air

In the second application shown in Fig. 4, the panel is baffled and laminated with an aluminium plate and a layer of melamine foam. The thicknesses of the plate and the melamine foam layer are 6 mm and 50 mm, and the width of the panel is 1 m. The plate is simply supported by the baffle but the frame of the melamine foam layer is fixed by the baffle. The properties of the melamine foam are listed in Tab. 1 and those of the plate are listed in Tab. 2 [22]. The mass per unit area of the plate is 16.2 kg/m^2 and that of the porous material layer is 0.55 kg/m^2, only 3.4% of the former. The plate is meshed with 3-noded 2.5D shell elements (with quadratic interpolation), the melamine foam is meshed with 8-noded 2.5D solid (with quadratic interpolation) elements and the panel/fluid interfaces on both sides of the panel are meshed with 3-noded 2.5D boundary elements (also with quadratic interpolation). Matching meshes, in which a node on an interface is common to domains sharing the interface, are used here and in the following application to a high-speed train floor structure. The mesh size of each element is about 15 mm, ensuring that in the plate, the solid frame, the saturated fluid and the external fluids there are at least 6 nodes per wavelength up to 6000 Hz. The following results are shown for a frequency range of 1 to 4000 Hz with a frequency

resolution of 1 Hz from 1 Hz to 99 Hz and 200 log-spaced points from 100 Hz to 4000 Hz.

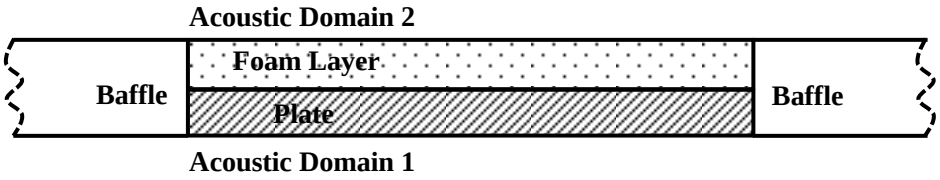

Fig. 4 A sketch of a baffled panel laminated with a plate and a melamine foam layer

Tab. 2 Material properties of the plate [22]

Young's modulus (Pa)	Density (kg/m^3)	Poisson's ratio	Loss factor
7.1×10^{10}	2.7×10^{3}	0.332	0.005

Results from the 2.5D FE-BE model and the TMM model are shown in Fig. 5. For comparison, the STL of the plate alone predicted using the 2.5D FE-BE model is also shown. Two incident angles are considered: ψ = 90 º and φ = 90 º (normal incidence, Fig. 5(a)) and ψ = 45 º and φ = 45 º (oblique incidence, Fig. 5(b)). It can be seen that TMM fails to predict the dips at about 14 Hz, 132 Hz and 366 Hz at which a new propagating wave cuts on in the plate. This is because TMM assumes an infinite width for the plate, preventing the plate from any modal behaviour. However, for frequencies above 132 Hz and well away from the cut-on frequencies of the plate, TMM can give sufficiently accurate predictions. This is because at these frequencies, the STL is mainly controlled by the mass of the panel. Below 14 Hz, the STL is mainly determined by the stiffness of the plate. For the normal incidence in Fig. 5(a), a dip at about 843 Hz is predicted and such a dip does not appear to the bare plate. This dip is due to the resonance of the solid frame of the melamine foam. The resonance frequency may be predicted with Eq. (65). In fact, with the parameters of the melamine foam listed in Tab. 1, Eq. (65) predicts a frequency at 834 Hz, close to the dip frequency. The dip at 2470 Hz is attributed to the high-order resonance of the solid frame. It will be demonstrated later in Fig. 6 that this dip disappears if an air gap is present between the plate and the melamine foam layer.

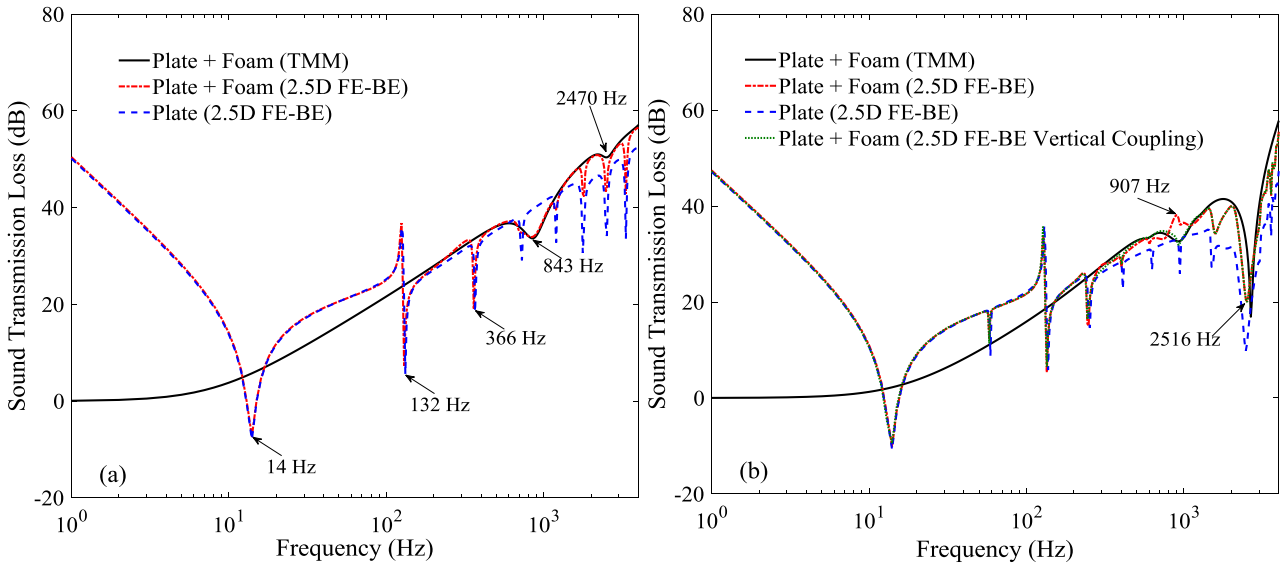

Fig. 5 STL predicted for a panel laminated with a 6 mm thick aluminium plate and 50 mm thick melamine foam. (a) Normal incidence (ψ = 90 º, φ= 90 º); (b) oblique incidence (ψ = 45 º, φ = 45 º).

For the oblique incidence in Fig. 5(b), the resonance frequency of the frame produces a peak instead of a dip that appears at 907 Hz. This is due to the presence of in-plane coupling at the interface of the plate with the melamine foam in the FE-BE model, which is not included in the TMM model. An additional result is shown with a green dotted curve, for which the in-plane coupling is suppressed; by doing so a dip instead of a peak is produced at 907 Hz. There is a deep dip at around 2516 Hz in Fig. 5(b). This is the coincidence freqeuncy of the panel at the associated incidence angle. However, the STL at this frequency is under-predicted by TMM, possibly due to the fact that the supports of the structure cannot be considered in TMM.

The application of the melamine foam layer can produce around 5-10 dB STL improvement for the plate above about 1000 Hz and 200 Hz for the normal and oblique incidences. By comparing the masses of the plate and the melamine foam layer, it can be concluded that the improvement is mainly contributed by the damping and absorption of the melamine foam layer.

Now it is assumed that there is a 1 mm air gap between the plate and the melamine foam layer shown in Fig. 4. STLs predicted using the 2.5D FE-BE model and TMM are compared in Fig. 6. For comparison, the 2.5D FE-BE prediction of the panel without the air gap and in-plane coupling is also plotted. For the two incident waves, the 2.5D FE-BE prediction generally agrees well with the TMM prediction for frequencies above about 132 Hz and well away from the cut-on modes of the plate. The dip at 843 Hz for the normal incidence and at 907 Hz for the oblique incidence, arising from the frame resonance, are suppressed by the air gap since now the vibration of the solid

frame of the melamine foam layer is decoupled from that of the plate. Above about 3000 Hz for the normal incidence and 2000 Hz for the oblique incidence, the 2.5D FE-BE prediction for the panel with the air gap and that without the air gap are almost the same. This may be explained by that the vibration of the porous material layer is dominated by air-borne waves in the interstitial fluid at high frequencies [7]. For an air-borne wave in the porous layer, motions of the solid frame and the interstitial fluid are decoupled, and the vibration amplitude of the fluid is much larger than that of the frame, keeping the frame almost motionless. This makes the two panels (one with the air gap and the other without) have similar STLs at high frequencies. The dip predicted with TMM at 2470 Hz noted in Fig. 5(a), due to the high-order resonance of the solid frame, also disappears by setting the air gap.

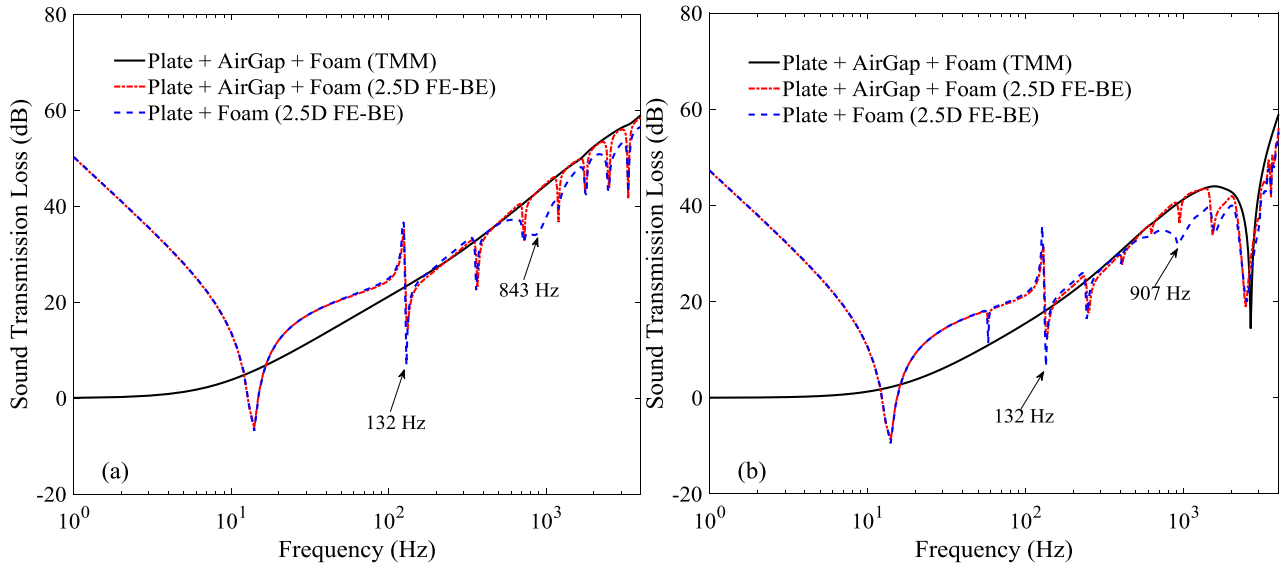

Fig. 6 STL predicted for the panel reconstructed by setting a 1 mm thick air gap between the plate and the melamine foam layer. (a) Normal incidence (ψ = 90 º, φ = 90 º); (b) oblique incidence (ψ = 45 º, φ = 45 º).

The results demonstrate that the elasticity of the solid frame has a great influence on the vibro-acoustics of the panel. Since the elasticity of the solid frame is neglected in Ref. [6] and the porous material layer is assumed to be acoustically thin and behave locally, it may cause significant errors.

The model developed recently in Ref. [26] may also be used to predict STL for panels similar to that shown in Fig. 4. In that model, the plate is also modelled using 2.5D FE-BE but the porous material layers are modelled using TMM (therefore these porous material layers have been assumed to be unbounded in the *x*-*y* plane), making the model much more efficient than the full 2.5D FE-BE model. Comparisons are also made in Ref. [26] between these two models, showing that at

sufficiently high frequencies, these two models give the same result. However, the one developed in Ref. [26] overestimates STL at low frequencies because the porous material layer is assumed to be extended infinitely in the *y*-direction, completely covering the baffles.

Now the panel discussed in Fig. 4 is redesigned by replacing the 50 mm thick melamine foam layer with two porous material layers, a 25 mm thick melamine foam layer overlaid by a 25 mm thick glass wool layer, as shown in Fig. 7. The application of two porous material layers is to test the coupling between two different porous media and to demonstrate the effect of such treatment on the STL of the panel. The mass per unit area of the melamine foam layer is 0.275 kg/m^2, only 1.7% of the plate, and that of the glass wool layer is 3.25 kg/m^2, about 20% of the plate. The results are shown in Fig. 8. For comparison, the 2.5D FE-BE prediction of the panel with 50 mm thick melamine foam layer, without considering the in-plane coupling, is also plotted. Material properties of the porous materials are listed in Tab. 1.

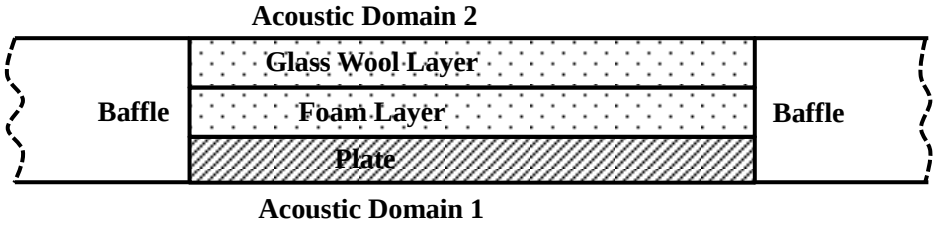

Fig. 7 A sketch of a baffled panel laminated with a plate and two poro-elastic layers

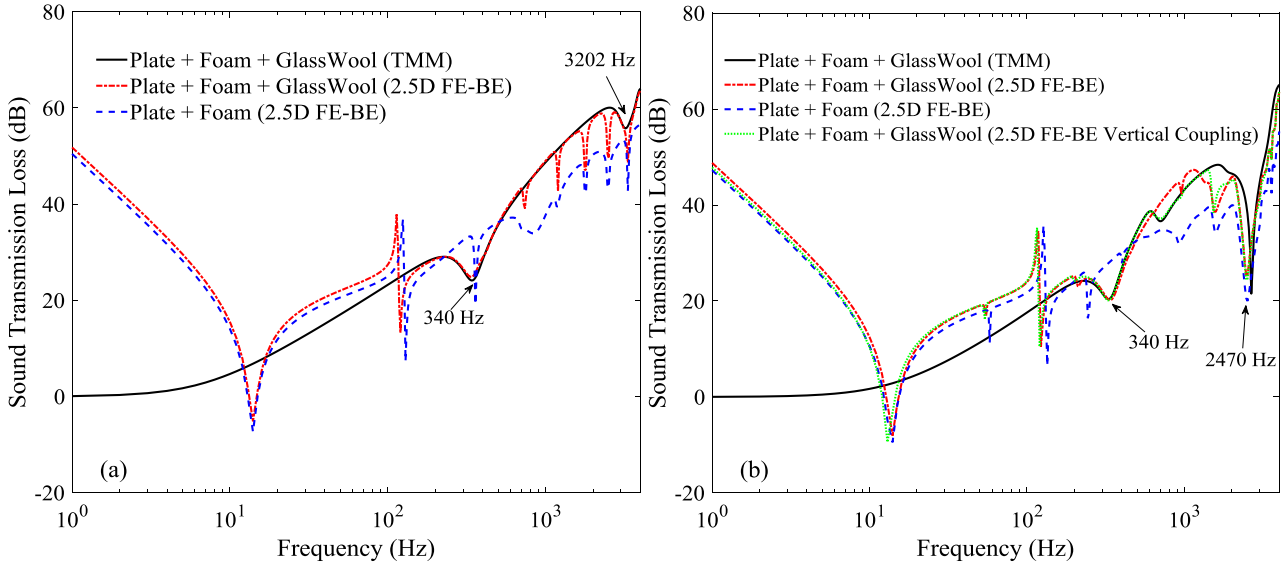

Fig. 8 STL predicted for a baffled panel laminated with a 6 mm thick aluminium plate, a 25 mm thick foam layer and a 25 mm thick glass wool layer. (a) Normal incidence (ψ = 90 º, φ = 90 º); (b) oblique incidence (ψ = 45 º, φ= 45 º).

For the normal incidence in Fig. 8(a), the dip occurring at 340 Hz predicted by both 2.5D

FE-BE and TMM is attributed to the mass-spring-mass (MSM) resonance of the system in which the plate and the heavier glass wool layer behave like masses, while the softer foam layer acts as a spring. According to Ref. [33], the MSM resonance frequency is given by

$$f_{\mathrm{MSM}} = \frac{1}{2\pi\cos\theta}\sqrt{\frac{k'\left(m_{\mathrm{p1}}+m_{\mathrm{p2}}\right)}{m_{\mathrm{p1}}m_{\mathrm{p2}}}}, \tag{67}$$

where m_{p1} and m_{p2} are the masses per unit area of the outer layers; θ is the incident angle defined in Fig. 1 (for normal incidence, $\theta = 0$); k' is the equivalent stiffness of the middle layer, which can be calculated approximately as

$$k' = \frac{K'_{\mathrm{c}}}{h}, \tag{68}$$

where h is the thickness of the layer and K'_{c} is the equivalent elastic constant of the compressional wave of the layer. For a porous material in which the fluid is constrained to move together with the frame at the boundaries, K'_{c} can be approximately evaluated by

$$K'_{\mathrm{c}} = \left(1-\phi\right)K_{\mathrm{c}}^{\mathrm{s}} + \phi K_{\mathrm{c}}^{\mathrm{f}}, \tag{69}$$

otherwise

$$K'_{\mathrm{c}} = \left(1-\phi\right)K_{\mathrm{c}}^{\mathrm{s}}, \tag{70}$$

where $K_{\mathrm{c}}^{\mathrm{s}}$ and $K_{\mathrm{c}}^{\mathrm{f}}$ are the corresponding elastic constants of the solid and the fluid. Since the interstitial fluid can flow across the interface of the two porous material layers, the equivalent stiffness should be estimated using Eqs. (68) and (70). Therefore, using the parameters of the melamine foam and glass wool listed in Tab. 1, Eq. (67) predicts the MSM resonance frequency at around 339 Hz, which is very close to the MSM resonance frequency noted in the figure. The dip occurring at 3202 Hz is caused by the standing wave of the solid frame in the softer foam layer.

For the oblique incidence in Fig. 8(b), above the MSM resonance frequency, where the motion of the plate is decoupled from that of the heavier glass wool layer, the 2.5D FE-BE results show a general agreement with TMM. An apparent difference exists between about 340 Hz and 2000 Hz. This is mainly attributed to the difference between the two models in coupling at the interface between the plate and the porous material layer; the FE-BE model includes the in-plane coupling whereas the TMM does not. The difference is reduced by removing the in-plane coupling at the interface as shown by a green dotted curve. This demonstrates the importance of including the

in-plane coupling.

It can also be found that above about 500 Hz, the plate with a soft melamine foam layer and a heavier upper glass wool layer can generate a higher STL than that when the plate is with a single melamine foam layer of the same thickness. This is due to the MSM resonance in the former configuration and this MSM resonance does not exist in the latter configuration. After the MSM resonance frequency, the vibration of the heavier upper layer is isolated from that of the plate by the soft middle melamine foam layer, leading to a more rapidly increasing STL.

4. Application to a high-speed train floor structure

In this section, the 2.5D FE-BE model is applied to study the vibro-acoustic behaviour of a high-speed train floor structure. The structure is shown in Fig. 9. It consists of a complex aluminium extrusion, porous material layers and a wooden floor. There are wooden beams supporting the wooden floor so that the wooden floor can bear much more loads. To investigate the effects of the various components of the structure on STL, this section is divided into three sub-sections. In Section 4.1, only the extrusion and porous material layers are considered, without the wooden floor and wooden beams. In Section 4.2, the wooden floor is added but without the supporting beams. And finally, in Section 4.3, the actual floor structure is investigated by adding the supporting beams.

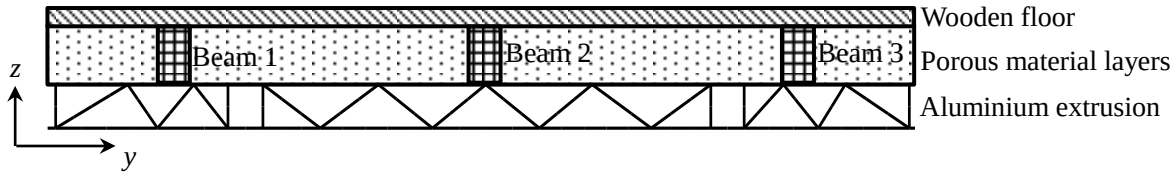

Fig. 9 A sketch of a composite floor structure used in high-speed trains

The width of the composite structure is 970 mm, the same width as those of samples used for STL measurement [24]. The extrusion is 50 mm thick and its material properties are the same as those of the plate listed in Tab. 2, Section 3. The upper and lower side boundaries of the extrusion along the infinitely long (*x*-) direction are simply supported, as shown in Fig. 10. The wooden floor is 20 mm thick. The two side boundaries along the *x*-direction are also simply supported. The Young's modulus, density, Poisson's ratio and loss factor of the wooden floor are listed in Tab. 3. There are three wooden beams within the width of the panel shown in Fig. 9. Beam 2 is at the centre width, and the distance between Beam 1 (3) and Beam 2 is 400 mm. The width of each beam is 40

mm, and the height is 60 mm [34]. Properties of the wooden beams are listed in Tab. 4. The cavity formed by the extrusion and the wooden floor is 60 mm thick and filled with porous materials (melamine foam or glass wool). The properties of the melamine foam and glass wool are listed in Tab. 1. The side surfaces of the porous layers interfacing with the baffle are fixed. The layers of porous material are fully coupled with the extrusion and the wooden floor by considering both the in-plane and out-of-plane motion at the interfaces. The air in the cavities of the extrusion is ignored since it has been shown to have negligible effect on the STL [25].

Tab. 3 Material properties of the wooden floor

Young's modulus (Pa)	Density (kg/m^3)	Poisson's ratio	Loss factor
2.7×10^9	730	0.3	0.06

Tab. 4 Properties of the wooden beams [34]

Young's modulus (Pa)	Density (kg/m^3)	Poisson's ratio	Loss factor
1×10^9	610	0.25	0.05

4.1 STL of the extrusion applied with layers of porous materials

The porous material layer can be a single layer of melamine foam, a single layer of glass wool or a combination of the two. The extrusion is meshed with 3-noded 2.5D shell elements with a maximum element size of 30 mm (Fig. 10). Each porous layer is meshed with 8-noded 2.5D solid elements with similar element sizes. The acoustic boundaries of the fluids on both sides of the structure are meshed with 3-noded 2.5D boundary elements with the same element size as that of the extrusion. The mesh size of the composite structure and the acoustic fluid domains ensures at least 6 nodes per wavelength up to about 3500 Hz. Full random incidences are assumed to predict the diffuse field STL with φ_{lim} and ψ_{lim} in Eq. (62) both being set to be 0° and with an integral step of 8°.

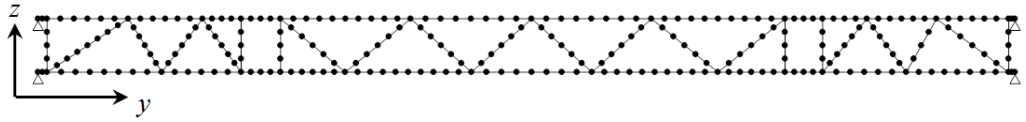

Fig. 10 Mesh and boundary condition of the aluminium extrusion

The predicted diffuse field STL is shown in Fig. 11. Results are shown for four different configurations of the porous layer, including a single layer of melamine foam, a single layer of glass

wool and two 30 mm layers of each in both sequences. It can be seen that attaching layers of porous material improves the STL of the extrusion above 200 Hz, with improvements of more than 10 dB. Below 200 Hz where the STL is determined by the stiffness of the composite structure, the porous material layers have negligible effect on STL of the extrusion. This is because that, the stiffness of the extrusion is much higher than the porous material layers and the sound absorption effect of the porous material layers are not significant at these low frequencies.

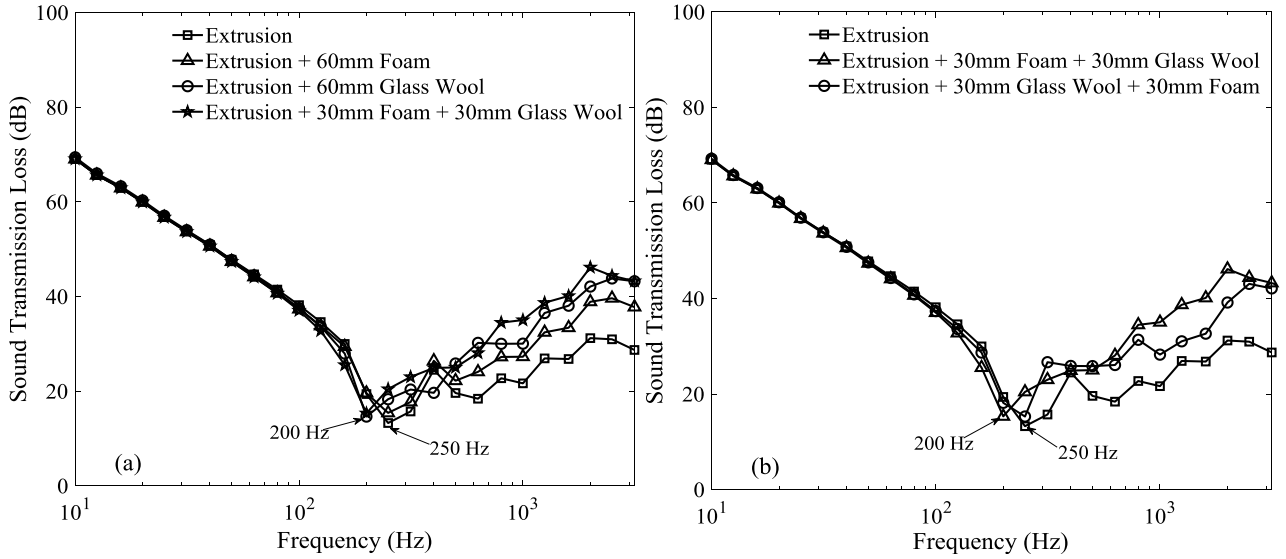

Fig. 11 Influence of porous layer configuration on the diffuse field STL of the extrusion in the absence of the wooden floor and wooden beams. (a) Influence of porous layer configuration; (b) Influence of porous layer sequence.

The single layer of glass wool can bring a greater benefit than a single layer of melamine foam since it has a relatively larger flow resistivity, mass and stiffness. The flow resistivity significantly affects the damping or dissipation mechanism between the interstitial fluid and the solid frame. The dip occurring at the 250 Hz third octave frequency band for the extrusion is due to the cut-on of the first propagating wave in the extrusion. As the glass wool has a much larger mass than the foam by about a factor of thirteen, the STL dip due to the cut-on of the propagating wave in the extrusion shifts from the 250 Hz to the 200 Hz frequency band, as shown in Fig. 11(a).

The treatment with two porous layers generates the highest STL, and the first dip also occurs in the 200 Hz frequency band. This dip is attributed to the resonance of the mass-spring-mass (MSM) system, in which the extrusion and the upper heavier glass wool layer act as the masses and the middle layer performs as the spring. As shown in Fig. 11(b), the alignment sequence of the two layers of porous materials has a significant influence on the STL of the composite structure. This is

because the porous layers arranged with a lighter lower layer (foam) and a heavier upper layer (glass wool) can produce the MSM resonance while it does not occur in the other arrangement sequence. The MSM resonance makes the foam/glass wool configuration have a higher STL than the glass wool/foam configuration above about 500 Hz.

4.2 STL improvement by adding the wooden floor

Now the wooden floor is added and is meshed with 2.5D shell elements with similar element size to that of the extrusion. The diffuse field STL of the composite structure is shown in Fig. 12. The porous layer configurations are the same as those considered in Section 4.1. It can be seen from Fig. 12(a) that the addition of the wooden floor further improve the STL by as much as 10-30 dB for frequencies higher than 200 Hz. The dips at 100 Hz, 125 Hz and 160 Hz in Fig. 12(a) are due to the cut-on of in-phase waves in the extrusion and the wooden floor. The in-phase waves in the composite structure cut on at around 103 Hz, 150 Hz and 166 Hz in narrow frequency band for, respectively, the single layer of foam, single layer of glass wool and the combination of their two. The cut-on frequencies of the corresponding out-of-phase waves are 240, 250 and 440 Hz. Since the glass wool is stiffer than the foam, filling the cavity with a single layer of glass wool makes these two dips occur at a higher frequency than that with a single layer of foam. Since the two porous layers behave like a connected spring, their combined stiffness lies between that of a single layer of foam and that of a single layer of glass wool, hence making these two dips occur between those of the latter two cases.

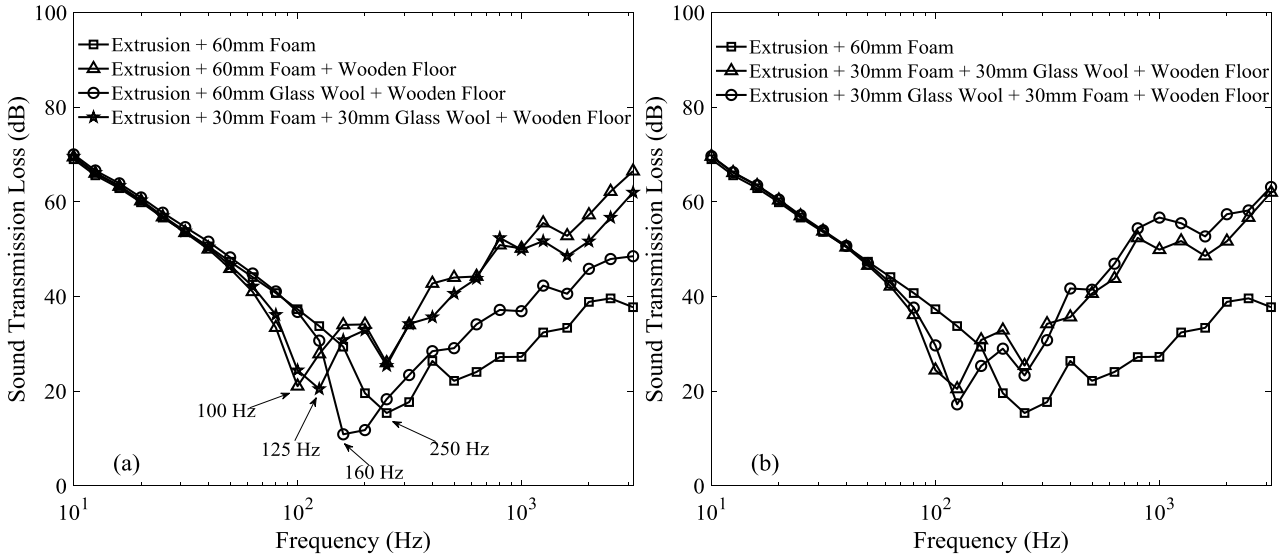

Fig. 12 Influence of porous layer configuration on diffuse field STL of the extrusion with presence of the wooden floor. (a) Influence of porous layer configuration; (b) Influence of porous layer sequence.

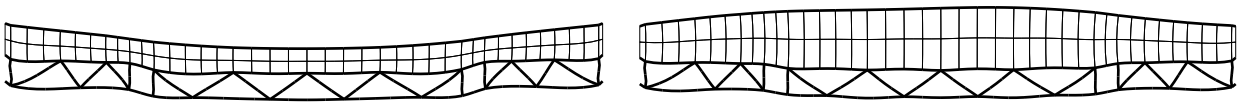

(a) (b)

Fig. 13 Cross-section shapes of the in-phase and out-of-phase cut-on waves in the composite structure with its cavity filled with a 60 mm thick layer of glass wool. (a) In-phase cut-on wave (at 166 Hz); (b) Out-of-phase cut-on wave (at 440 Hz).

The cut-on frequency of the out-of-phase wave corresponds to the MSM resonance frequency. The cross-section shapes of the in-phase and out-of-phase cut-on waves for the single layer of glass wool are shown in Fig. 13. Below the MSM resonance frequency the extrusion and the wooden floor vibrate together, whereas their motions are isolated above this frequency. Above the MSM resonance dip frequency the STL rise rapidly. Therefore, filling the cavity with a single layer of foam generates the highest STL above the MSM resonance frequency, while that with two porous layers produces the second highest STL, and that with a single layer of glass wool gives the third highest STL.

As shown in Fig. 12(b), the alignment sequence of the two layers of porous materials has little influence on the STL of the composite structure, since the stiffness of the connected spring does not change with the alignment sequence.

4.3 Effect of adding the supporting beams

Now the three supporting beams shown in Fig. 9 are added, forming the actual structure. The beams can also be modelled with the 2.5D FE method, while here for simplicity, they are treated as vertical and bending springs in the longitudinally vertical plane (the *x*-*z* plane), without considering the mass of the wooden beams. This is reasonable since the mass of the three beams is much less than that of the extrusion and the wooden floor. The stiffness of the vertical spring per unit length in the *x*-direction, k_{ts}, and that of the bending spring, k_{rs}, are given by

$$k_{\mathrm{ts}} = \frac{E_{\mathrm{s}} b_{\mathrm{s}}}{h_{\mathrm{s}}}, \tag{71}$$

$$k_{\mathrm{rs}} = \frac{E_{\mathrm{s}} h_{\mathrm{s}}^3 b_{\mathrm{s}}}{12}, \tag{72}$$

where E_{s} is the Young's modulus, b_{s} is the width and h_{s} is the height of the beam. The springs will produce coupling stiffness matrices, $\mathbf{K}_{\mathrm{ts}}$ and $\mathbf{K}_{\mathrm{rs}}$, to the coefficient matrix of the 2.5D FE-BE

governing equation, i.e. Eq. (55), while not increase the total degrees of freedom of the model.

From Fig. 9 it can be seen that four cavities are formed by the extrusion, the wooden floor and the three beams as well as the baffles. To investigate the effect of cavity content on STL, the cavities are alternatively assumed to be vacuum, filled with air, or with melamine foam. The predicted STLs are compared in Fig. 14(a). It can be seen that, below 100 Hz, the cavity content almost has no effect on STL, since at these frequencies, STL is dominantly determined by the stiffness of the structure while the cavity content does not significantly influence the stiffness. Filling air in the cavities makes no difference for all the frequencies considered. However, filling the cavities with melamine foam does have some effect on STL of the structure. Around the dip frequency, it causes up to 5 dB decrease in STL. These frequencies are well lower than the resonance frequency of the melamine foam frame and the foam behaves like distributed springs, strengthening energy flow from the extrusion to the wooden floor. However, for frequencies higher than about 600 Hz, a few dB improvements are achieved by completely filling the cavities with melamine foam. This may be explained by the damping increased by the melamine foam.

It should be noted that the above observations change if the stiffness of the supporting beams is much reduced, as demonstrated in Fig. 14(b) for which the Young's modulus of the wooden beam is reduced by a factor of one hundred. Below about 125 Hz, where the STL is mainly controlled by the stiffness of the complete structure, filling the cavities with melamine foam or air can bring a little STL benefits. However, from about 125 Hz to 250 Hz, presence of media (air or melamine foam) in the cavities reduces the STL of the structure by about 5-10 dB. This is attributed to the same mechanism as described in Fig. 14(a), that the filling media can strengthen energy flow between the two outer panels. Above about 250 Hz, the structure with cavities filled with air performs worst due to the standing waves in the air. The damping increased by the melamine foam can improve the STL by about 5 dB at these frequencies. However, filling the cavities with melamine foam makes little difference in STL of the structure from about 250 Hz to 1250 Hz. At higher frequencies, filling cavities with melamine foam reduces STL by about 5 dB. This is caused by the standing waves in the interstitial fluid of the melamine foam.

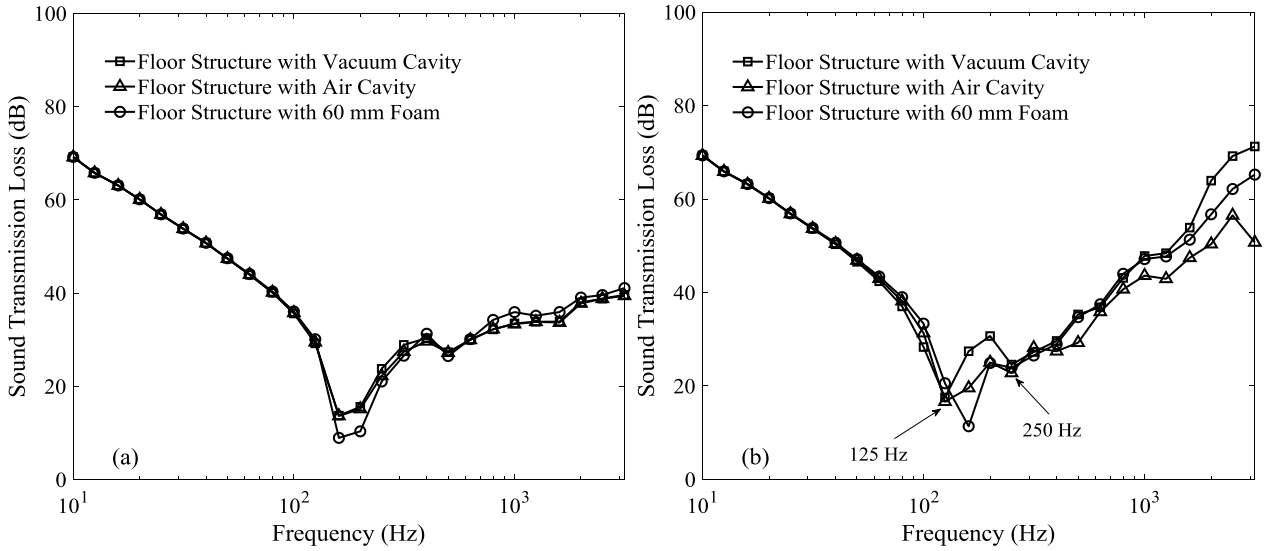

Fig. 14 STLs of the complete floor structure. (a) Original wooden beam; (b) Young's modulus of the wooden beam is reduced by a factor of one hundred.

5. Conclusions

In this paper, a 2.5D FE model for poro-elastic media and its coupling with 2.5D FE models of solids and other poro-elastic media, as well as 2.5D FE/BE models of fluids, are derived. This generates a 2.5D FE-BE model which can be used to study the vibro-acoustic behaviour of panels complicated by co-existence of solids, fluids and poro-elastic media. The model is applied to several multi-layered panels for which TMM may also be applied at high frequencies. It turns out that the model proposed in this paper agrees well with TMM in the mass-controlled frequency region and above, demonstrating the accuracy of the proposed model. Results show that the elasticity of the solid frame of a porous medium has a significant effect on the vibro-acoustics of the multi-layered panel containing porous media.

The model is then applied to investigate the STL of a composite floor structure used in railway vehicles. Results show that if the wooden floor is just floated on layers of porous materials, then the porous materials can greatly improve STL. Arrangement of the porous material layers can have a significant effect. However, if there are supporting beams between the wooden floor and the extrusion, the importance of these porous material layers is much reduced in terms of sound insulation. A careful design of the porous material layers is needed for vibro-acoustics.

It should be pointed out that the model is formulated based on the condition that the structure is uniform and infinitely long in the *x*-direction. Although it is well accepted that such a modelling approach is applicable to structures which are uniform but of finite length in *x*-direction at

frequencies at which the structural and acoustical wavelengths are much shorter than the lengths of the structures, a more quantitative and useful rule is desired for determining when a vibro-acoustic structure of finite length can be replaced with an infinitely long one so that the 2.5D FE-BE model can be applied.

Acknowledgements

This work is funded by the National Key R&D Program of China (2016YFE0205200) and the National Natural Science Foundation of China (U1834201).

References

[1] I.I. Beranek, I.L. Vér, Noise and Vibration Control Engineering: Principles and Applications, second ed., Wiley, 2005.

[2] F. Xin, T. Lu, Sound radiation of orthogonally rib-stiffened sandwich structures with cavity absorption, Compos. Sci. Technol. 70 (2010) 2198-2206. (DOI: 10.1016/j.compscitech.2010.09.001)

[3] T. Fu, Z. Chen, H. Yu, Z. Wang, X. Liu, An analytical study of sound transmission through corrugated core FGM sandwich plates filled with porous material, Compos.: Part B 151 (2018) 161-172. (DOI: 10.1016/j.compositesb.2018.06.010)

[4] H. Qian, Z. He, W. Jiang, W. Peng, Sound transmission of periodic composite structure lined with porous core: Rib-stiffened double panel case, J. Sound Vib. 440 (2019) 256-276. (DOI: 10.1016/j.jsv.2018.10.029)

[5] D. Wang, M. Li, Z. Wen, Sound transmission through a sandwich structure with two layered pyramidal core and cavity absorption, J. Sound Vib. 459 (2019) 114853. (DOI: 10.1016/j.jsv.2019.114853)

[6] S. Zhang, X. Sheng, Analysis of sound transmission loss of a rectangular plate with acoustic treatments, Proc. of ISMA and USD, (2018) 725-740.

[7] J.-F. Allard, N. Atalla, Propagation of Sound in Porous Media, second ed., Wiley, 2009.

[8] A. Craggs, A finite element for rigid porous absorbing materials, J. Sound Vib. 61 (1978) 101-111. (DOI: 10.1016/0022-460X(78)90044-5)

[9] R. Panneton, N. Atalla, Numerical prediction of sound transmission through multilayer systems with isotropic poroelastic materials, J. Acoust. Soc. Am. 100(1996) 346-354. (DOI: 10.1121/1.415956)

[10] R. Panneton, N. Atalla, An efficient finite element scheme for solving the three-dimensional poroelasticity problem in acoustics, J. Acoust. Soc. Am. 101 (1997) 3287-3298. (DOI: 10.1121/1.418345)

[11] Y.J. Kang, J.S. Bolton, Finite element modelling of isotropic elastic porous materials coupled with acoustical finite elements, J. Acoust. Soc. Am. 98(1995) 635-643. (DOI: 10.1121/1.414357)

[12] Y.J. Kang, J.S. Bolton, A finite element model for sound transmission through foam-lined double-panel structures, J. Acoust. Soc. Am. 99(1996) 2755-2765. (DOI: 10.1121/1.414856)

[13] J.P. Coyette, H. Wynendaele, A finite element model for predicting the acoustic transmission characteristics of layered structures, Proc. of Inter-Noise, 1995.

[14] M.A. Biot, The theory of propagation of elastic waves in a fluid-saturated porous solid. I. Low-frequency range, J. Acoust. Soc. Am. 28(2) (1956) 168-178. (DOI: 10.1121/1.1908239)

[15] M.A. Biot, Theory of propagation of elastic waves in a fluid-saturated porous media. II. Higher-frequency range, J. Acoust. Soc. Am. 28(2) (1956) 179-191. (DOI: 10.1121/1.1908241)

[16] N. Atalla, R. Paneton, P. Debergue, A mixed displacement pressure formulation for Biot's poroelasticity equations, 131st meeting of the A.S.A., Indianapolis.

[17] S. Gorog, R. Paneton, N. Atalla, Mixed displacement-pressure formulation for acoustic anisotropic open porous media, J. Appl. Phys. 82(1997) 4192-4196. (DOI: 10.1063/1.366221)

[18] N. Atalla, R. Paneton, P. Debergue, A mixed displacements-pressure formulation for poroelastic materials, J. Acoust. Soc. Am. 104(3) (1998) 1444-1452. (DOI: 10.1121/1.424355)

[19] N. Atalla, M.A. Hamdi, R. Panneton, Enhanced weak integral formulation for the mixed (**u**,p) poroelastic equations, J. Acoust. Soc. Am. 109(6) (2001) 3065-3068. (DOI: 10.1121/1.1365423)

[20] P. Debergue, R. Panneton, N. Atalla, Boundary conditions for the weak formulation of the mixed (**u**,p) poroelasticity problem, J. Acoust. Soc. Am. 106(5) (1999) 2383-2390. (DOI: 10.1121/1.428075)

[21] U. Orrenius, S. Finnveden, Calculation of wave propagation in rib-stiffened plate structures, J. Sound Vib. 182 (1996) 203-224. (DOI: 10.1006/jsvi.1996.0565)

[22] I. Prasetiyo, Investigation of Sound Transmission in Lightweight Structures Using a waveguide Finite Element/Boundary Element Approach, PhD thesis, University of Southampton, 2012.

[23] C.M. Nilsson, A.N. Thite, C.J.C. Jones, D.J. Thompson, Estimation of sound transmission through extruded panels using a coupled waveguide finite element-boundary element method, Proc. of IWRN, 2007. (DOI: 10.1007/978-3-540-74893-9_43)

[24] Y. Zhang, D.J. Thompson, G. Squicciarini, J. Ryue, X. Xiao, Sound transmission loss properties of truss core extruded panels, Appl. Acoust. 131 (2018) 134-153. (DOI: 10.1016/j.apacoust.2017.10.021)

[25] H. Kim, J. Ryue, D.J. Thompson, A.D. Müller, Application of a wavenumber domain numerical method to the prediction of the radiation efficiency and sound transmission of complex extruded panels, J. Sound Vib. 449 (2019) 98-120. (DOI: 10.1016/j.jsv.2019.02.036)

[26] T. Deng, M. Li, S. Zhang, X. Sheng, D.J. Thompson, Combining the 2.5D FE-BE method and the TMM method to study the vibro-acoustics of acoustically treated rib-stiffened panels, J. Sound Vib. 493 (2021) 115825. (DOI: 10.1016/j.jsv.2020.115825)

[27] H. Jeong, A numerical investigation of noise mitigation for railway track, PhD thesis, University of Southampton, 2018.

[28] C.M. Nilsson, J. Ryue, C.J.C. Jones, Theory manual for WANDS 2.1 wavenumber domain FE-BE software for structures and fluids, University of Southampton, 2010.

[29] X. Sheng, T. Zhong, Y. Li, Vibration and sound radiation of slab high-speed railway tracks subject to a moving harmonic load, J. Sound Vib. 395 (2017) 160-186. (DOI: 10.1016/j.jsv.2017.02.024)

[30] D.L. Johnson, J. Koplik, R. Dashen, Theory of dynamic permeability and tortuosity in fluid-saturated media, J. Fluid Mech. 176 (1987) 379-402. (DOI: 10.1017/S0022112087000727)

[31] Y. Champoux, J.F. Allard, Dynamic tortuosity and bulk modulus in air-saturated porous media, J. Appl. Phys. 70 (1991) 1975-9. (DOI: 10.1063/1.349482)

[32] L. Beranek, Noise and Vibration Control, McGraw-Hill, 1971.

[33] J. Wang, T. Lu, J. Woodhouse, et al, Sound transmission through lightweight double-leaf partitions: theoretical modelling, J. Sound Vib. 286(4-5) (2005) 817-847. (DOI: 10.1016/j.jsv.2004.10.020)

[34] J. Zhang, D. Yao, R. Wang, X. Xiao, Vibro-acoustic modelling of high-speed train composite floor and contribution analysis of its constituent materials, Compos. Struct. 256 (2021) 113049.

(DOI: 10.1016/j.compstruct.2020.113049)